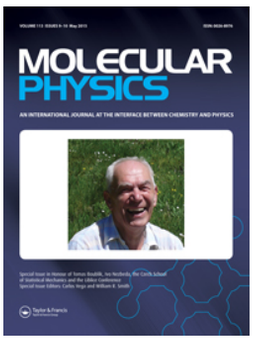

Taylor & Francis
Taylor & Francis Group

Molecular Physics

An International Journal at the Interface Between Chemistry and Physics

ISSN: 0026-8976 (Print) 1362-3028 (Online) Journal homepage: https://www.tandfonline.com/loi/tmph20

SAFT-γ force field for the simulation of molecular fluids: 4. A single-site coarse-grained model of water applicable over a wide temperature range

Olga Lobanova, Carlos Avendaño, Thomas Lafitte, Erich A. Müller & George Jackson

To cite this article: Olga Lobanova, Carlos Avendaño, Thomas Lafitte, Erich A. Müller & George Jackson (2015) SAFT-γ force field for the simulation of molecular fluids: 4. A single-site coarse-grained model of water applicable over a wide temperature range, Molecular Physics, 113:9-10, 1228-1249, DOI: 10.1080/00268976.2015.1004804

To link to this article: https://doi.org/10.1080/00268976.2015.1004804

Published online: 31 Mar 2015.

Molecular Physics, 2015
Vol. 113, Nos. 9–10, 1228–1249, http://dx.doi.org/10.1080/00268976.2015.1004804

Taylor & Francis
Taylor & Francis Group

INVITED ARTICLE

SAFT-γ force field for the simulation of molecular fluids: 4. A single-site coarse-grained model of water applicable over a wide temperature range

Olga Lobanova[a], Carlos Avendaño[a,b], Thomas Lafitte[a,c], Erich A. Müller[a] and George Jackson[a,*]

[a]*Department of Chemical Engineering, Centre for Process Systems Engineering, Imperial College London, South Kensington Campus, London SW7 2AZ, United Kingdom;* [b]*School of Chemical Engineering and Analytical Sciences, The University of Manchester, Manchester M13 9PL, United Kingdom;* [c]*Process Systems Enterprise Ltd, London W6 7HA, United Kingdom*

(*Received 20 November 2014; accepted 29 December 2014*)

In this work, we develop coarse-grained (CG) force fields for water, where the effective CG intermolecular interactions between particles are estimated from an accurate description of the macroscopic experimental vapour–liquid equilibria data by means of a molecular-based equation of state. The statistical associating fluid theory for Mie (generalised Lennard-Jones) potentials of variable range (SAFT-VR Mie) is used to parameterise spherically symmetrical (isotropic) force fields for water. The resulting SAFT-γ CG models are based on the Mie (8-6) form with size and energy parameters that are temperature dependent; the latter dependence is a consequence of the angle averaging of the directional polar interactions present in water. At the simplest level of CG where a water molecule is represented as a single bead, it is well known that an isotropic potential cannot be used to accurately reproduce all of the thermodynamic properties of water simultaneously. In order to address this deficiency, we propose two CG potential models of water based on a faithful description of different target properties over a wide range of temperatures: our CGW1-vle model is parameterised to match the saturated-liquid density and vapour pressure; our other CGW1-ift model is parameterised to match the saturated-liquid density and vapour–liquid interfacial tension. A higher level of CG corresponding to two water molecules per CG bead is also considered: the corresponding CGW2-bio model is developed to reproduce the saturated-liquid density and vapour–liquid interfacial tension in the physiological temperature range, and is particularly suitable for the large-scale simulation of bio-molecular systems. A critical comparison of the phase equilibrium and transport properties of the proposed force fields is made with the more traditional atomistic models.

Keywords: aqueous systems; molecular simulation; interfacial properties; force fields

1. Introduction

Water is perhaps the most important liquid in nature and is the most common solvent in biological and industrial systems. Despite an enormous research effort that spans over more than a century, modelling aqueous systems still remains a challenge [1]. A reliable force field is crucial for an accurate description of the properties of water and its mixtures. Numerous intermolecular potential models have been developed at different levels of resolution by matching specific structural and/or thermodynamic properties. Without the intension of being exhaustive, it is important to briefly acknowledge some of the popular intermolecular potential models for water. The reader is directed to the excellent reviews on the development of force fields for water based on: a quantum-level description [2–4]; a classical atomistic description [5–9], including a particular focus on polarisable models [10]; a coarse-grained (CG) representation [11–15]; and a critical experimental validation of the various models, including the corresponding anomalies in the structural, thermodynamic, and dynamical properties [16,17].

In first-principles quantum mechanical approaches, the total potential energy surface of the system is determined by solving the Schrödinger equation using the Born–Oppenheimer approximation. As a result of the computational complexity, these calculations are restricted to relatively small clusters of water molecules. Furthermore, many of the predicted bulk thermodynamic properties are only in qualitative agreement with experimental observables [3,4]. One of the best known force fields obtained by parameterising *ab initio* quantum mechanical calculations of the water dimer in different relative molecular positions and orientations is the Matsuoka–Clementi–Yoshimine (MCY) model [18]. Although the structural properties are well reproduced with the MCY model, significant deviations are observed for the liquid density. Car and Parrinello [19] combined traditional molecular-dynamics (MD) simulation with quantum density functional theory (DFT) in their seminal paper to simulate the fluid properties of water, explicitly introducing the electronic degrees of freedom as dynamical variables rather than using Born–Oppenheimer MD where the electron density is solved at each iteration.

* Corresponding author. Email: g.jackson@imperial.ac.uk

The quality of the description of the macroscopic behaviour largely depends on the the choice of functional and basis set used in the quantum simulation [20,21]. The vapour–liquid coexistence properties, which are particularly sensitive to details of the computation and the treatment of the dispersion interaction, can be different from the experimental values by several orders of magnitude [3,22,23]. An accurate first-principles DFT simulation of water still remains a challenge where the commonly employed forms of the exchange-correlation functional can lead to serious discrepancies in the prediction of some of the properties (including the structure, density, and internal energy) of the condensed liquid state [24]. Notwithstanding, the methodology makes it possible to predict the properties of clusters of over 100 molecules, allowing for an exploration of dense fluids [25,26].

At the classical atomistic level of description, experimental data for the bulk-phase thermophysical and structural properties are typically used to parameterise empirical pairwise additive potentials. These force fields make use of analytical functions providing a simplified classical representation of the repulsive, dispersive, and electrostatic interactions. Rigid non-polarisable models with partial point charges are commonly employed in this context. The classical intermolecular force fields of water in modern use are invariably based on the distributed-charge Lennard-Jones (LJ) models proposed by Bernal and Fowler [27], Rowlinson [28,29], Pople [30], and Bjerrum [31]. The first atomistic molecular simulation study of water was reported by Barker and Watts [32], who used the model of Rowlinson [29] in their Monte Carlo simulations. The Rowlinson model consists of a LJ spherical site and four electrostatic charges positioned to reproduce the dipole moment of water. A similar description has been used in subsequent studies to develop more reliable models with differing numbers of charged sites and geometries, including the BNS model of Ben-Naim and Stillinger [33], the ST2 model of Stillinger and Rahman [34,35], the simple point charge (SPC) models of Berendsen and co-workers [36–38], and the transferable interaction potential (TIP) models based on the work of Jorgensen and co-workers [8,39–47]; in this context, it is also important to mention the related distributed-charge exp-6 model of Errington and Panagiotopoulos [48], which is based on the modified Buckingham exponential-6 potential.

The SPC and TIP families of classical atomistic force fields generally offer a good overall description of the physical behaviour of water, even though they cannot be used to capture all of the properties and anomalies simultaneously [5,7]. For instance, the TIP4P model allows one to represent the overall phase diagram only qualitatively [49,50], and the predicted dielectric constant is highly underestimated compared to experiment [7]. The SPC, SPC/E, TIP3P, and TIP4P models are unable to provide one with an accurate representation of the experimental oxygen–oxygen radial distribution function [38,51,52], and unphysical clusters can be found in the gas phase with the TIP3P model [53]. The SPC, TIP3P, and TIP4P models underestimate the experimental melting temperature of water (273 K), with values of 190, 146, and 232 K, respectively [7]. An unsatisfactory description of the overall vapour–liquid equilibria, particularly the vapour pressure and second-virial coefficient, is generally found with the various SPC and TIP parameterisations [54–56]. As a consequence the values predicted for the normal boiling temperature of water can range from 364 and 368 K for the TIP4P and SPC models to 398 and 401 K for the SPC/E and TIP4P/2005 models, compared to the experimental value of 373 K; in cases where the boiling point is not reported, it can be estimated from a Clausius–Clapeyron analysis of the vapour pressures reported in Refs. [54] and [55]. Despite some of these inadequacies, the SCP and TIP point-charge models of water are still in ubiquitous use as they provide a predictive platform for a broad variety of properties, including complex aqueous systems of biomolecules at manageable computational expense. The best overall current description of the thermodynamic and structural properties of water (with classical non-polarisable force fields of this type) is achievable with the TIP4P/2005 (condensed liquid) and TIP4P/Ice (solid state) offerings [8,45,46]; the recently re-parameterised TIP4P model of Huang *et al.* [47] also yields a particularly good description of the saturation pressure and heat of vaporisation, including the near critical region.

Polarisable force fields first introduced in the late 1970s [57,58], and developed extensively since, account for the many-body polarisation effects in order to improve the description of the dielectric properties by, for example, including polarisable Gaussian charges [59–64], fluctuating charges [65,66], polarisable point charges and multipoles [67–71], moving charged shells [72], or molecular flexibility [73–75]. Taking many-body electrostatic effects into account also allows one to reproduce the properties of the low-density vapour and high-density liquid states of water simultaneously (see, for example, the work of Paricaud *et al.* [60]) as well as the anomalous behaviour characteristic of aqueous systems (e.g., Ref. [76]). Though certainly the way forward in terms of an improved overall description of the structure and thermodynamic properties of water and other polar fluids, the use of polarisable models comes, however, at the expense of added complexity and computational cost. Their application in large-scale simulations such as those required for dilute aqueous solutions of surfactants or biomacromolecules is extremely time intensive even with state-of-the-art hardware.

Less physically detailed potential models can be considered that do not incorporate the electrostatic interactions explicitly. Before we describe the use of CG methodologies to develop simple, typically spherically symmetrical, intermolecular potentials for water and aqueous systems designed to provide an accurate quantitative representation

of target structural and thermodynamic properties, it is important to acknowledge the large body of work on related so-called 'toy models'. In contrast to CG force fields, toy models are employed to capture the underlying qualitative physics of the interactions in water with the aim of representing distinctive features of the system's behaviour, such as the anomalous low density of ice, the density maximum, and the heat capacity and compressibility minima, without attempting to reproduce the properties faithfully. One of the first toy models of water of this type was developed by Ben-Naim [77] based on a LJ molecular core with directional attractive sites characterised by an angular-dependent Gaussian cut-off; two dimensional 'Mercedes-Benz' and three dimensional variants of the Ben-Naim model have now been used to help understand the qualitative features of the anomalous behaviour of water [12,78,79]. Other simple force fields have also been employed in this context, including isotropic models with two characteristic length scales, related core-softened potentials, and modified van der Waals models [80–96]. A quantitative description of some of the key thermodynamic properties of water can also be obtained with simple sticky-patch potentials which mimic the strong and short-range directional hydrogen bonding in water by including a number of off-centre sites within the spherical molecular core (see the review by Nezbeda [97], and references therein). A particularly good example of the development of sticky-patch models of water is the use of the statistical associating fluid theory (SAFT) to parameterise a force field for the simulation of confined systems [98], where the use of Ewald summations for the evaluation of the long-range electrostatic interactions can be problematic [99].

Modelling the water molecule as a single spherically symmetrical CG interaction site is, of course, a considerable challenge, because the strong anisotropy and short-ranged nature of the interactions are represented in a highly simplified, effective manner. The use of simple CG models of water without an explicit treatment of the electrostatics has nevertheless gained much popularity in recent years, driven by the need to simulate increasingly large systems for longer times [11–15,100–127]. It comes as no surprise to find that these simple isotropic models cannot be used to simultaneously reproduce all of the thermodynamic and structural properties of water. Despite the shortcomings due to the rather crude representation of the real force field, these CG models are very useful in the simulation of large macroscopic systems dominated by solvent effects, including biological systems and solvent-mediated microphase separation. The use of a simplified CG model offers a great saving in computational time and is therefore paramount as a platform for multiscale modelling. The main purpose of a CG model is to reproduce basic structural, dynamical, thermodynamic, and phase-equilibrium properties in reasonable agreement with the target experimental data, but at a low comparative computational cost. It is clear that by reducing the resolution through the CG procedure, one's capability of accurately describing the behaviour of the system must be diminished with respect to the atomistic models, which fail to faithfully reproduce some of the properties of interest. The key to a successful CG procedure is to establish the correct balance between simplicity and accuracy.

Coarse-grained models of water are commonly developed by lumping together several molecular features or molecules into a single CG bead. Different levels of CG mapping have been employed in this regard depending on the purpose of study, ranging from one [100] to five [118] water molecules per bead. Hadley and McCabe [115] have investigated different levels of CG of water, using a *K*-means algorithm to identify the spacial coordinates and the number of molecular clusters k in the system. In this manner, the most appropriate average number of water molecules per CG bead could be estimated. Hadley and McCabe concluded that a four-to-one mapping represents the best balance between accuracy and computational efficiency in the case of water. However, an inherit problem with the aggressive CG of several molecules into a single bead is that much of the molecular identity is lost; molecular details of interfacial densities and configurations are smeared out and crucially the vapour phase and properties associated with vapour–liquid equilibria become ill-defined.

With CG force fields, the electrostatics and hydrogen-bonding interactions are treated implicitly by considering an average, effective spherically symmetrical potential of mean force (PMF), which by its very nature is state dependent. 'Bottom-up techniques such as force matching [104] or iterative Boltzmann inversion (IBI) [109] have been used to parameterise the CG potentials of water from a detailed atomistic description. Some empirical CG water models have also been developed from a 'top-down' perspective: in such an approach, the parameters that characterise the potential functions are adjusted to match one or more target macroscopic properties using an iterative procedure. One of the most commonly employed empirical CG models is the MARTINI CG force field [103,107], based on the ubiquitous LJ (12-6) potential (with additional point charges for the interactions between charged groups) parameterised to represent the free energies of vaporisation, hydration, and partitioning between water and the hydrophobic component. The MARTINI model has been used to capture some of the salient structural properties of aqueous systems comprising lipids [103,128–130], surfactants [131–134], carbohydrates [135], and proteins [136–140], and as a consequence the force field has gained popularity in studies involving biomolecules. The MARTINI representation of water has a high computational efficiency as a result of the 'aggressive' level of CG, namely four water molecules per CG LJ bead. The strong polar interactions present in water and aqueous systems are represented with deep energetic

wells, which can unfortunately cause freezing at physiological temperatures [111,113], making the model suitable only for the simulation of mixtures with other components (that also act as anti-freeze agents). Furthermore, the use of the MARTINI force field can lead to a significant underestimate of the vapour–liquid interfacial tension and an overestimate of the compressibility of the solution [112].

A more faithful representation of the properties of water can be achieved by employing the softer Mie (generalised LJ) or Morse potentials along with a refinement of the model parameters, as suggested by He *et al.* [112] and Chiu *et al.* [113]. In earlier work on aqueous solutions of phospholipids, Shelley *et al.* [101] had already developed a CG model of water based on a three-to-one mapping scheme to study the self-assembly of the system. Their model is based on a soft-core interaction characterised by the Mie (6-4) potential, thereby avoiding the issue of premature freezing. Subsequently, He *et al.* [112] assessed several models at various levels of CG ranging from one to four molecules per bead using different Mie and Morse potentials. Klein and co-workers have now undertaken an extensive body of work employing soft-core potentials of this type to simulate the properties of aqueous solutions of ionic and non-ionic surfactants [105,141–144], ionic liquids [145], nanotubes [146], lipids [147,148], amino acids [149], and membranes [150]. In the case of the interaction between water molecules, the Mie CG models are typically parameterised empirically to reproduce the liquid density, compressibility, and interfacial tension at ambient temperature; inevitably, it is impossible to describe all three properties simultaneously at this level of CG. As we will also show later in our paper, one is not able to accurately predict vapour–liquid equilibrium properties such as the vapour pressure, vaporisation enthalpy, or heat capacity with such a parameterisation.

Freeing themselves of the restriction of a spherically symmetrical form of interaction, Molinero and co-workers [110,127] have proposed the monatomic water (mW) CG model based the on the Stillinger–Weber two- and three-body potential of silicon that favours a tetrahedral coordination of the molecules. The model was parameterised to match the experimental vaporisation enthalpy, melting point, and density of liquid water at ambient conditions, and with it, one retains the capability of describing some of the key structural properties, such as radial and angular distribution functions. Unfortunately, the mW model incorporates three-body contributions, which are costly to compute.

In our current work, we first focus on the development of simple isotropic CG force field for water based on a one-to-one mapping. We take a leaf out of the book of Klein and co-workers [101,105,112] and employ a Mie form of interaction, allowing the exponents to differ from the more usual LJ (12-6) prescription. The target thermodynamic properties in our case are the saturated-liquid density, the vapour pressure, and the vapour–liquid interfacial tension. The intermolecular parameters of the Mie potential are adjusted to provide an optimal description of the target properties. In contrast to the work of Klein and co-workers, we ensure that a good description is obtained over a wide temperature range; this is achieved by introducing a temperature dependence for the size and energy parameters of the model. In essence, our CG Mie force field for water represents a simple temperature-dependent PMF that can be used to faithfully describe the thermodynamic properties for a broad range of gaseous and condensed states. Other levels of CG are also considered within the SAFT-VR/SAFT-γ Mie framework as described in Section 3.5. Prototypical examples of molecular CG models of water are illustrated in Figure 1.

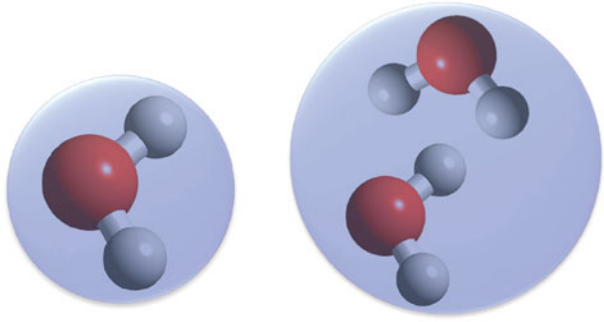

Figure 1. Coarse-grained molecular models for water, based on the one-to-one and two-to-one level of representation.

2. Methodology

2.1. SAFT-γ Mie force field

The interactions between water molecules is represented with a single CG spherical site interacting via the Mie potential [151]. The Mie potential is more versatile than the fixed LJ (12-6) form because the repulsive and attractive exponents can be varied independently to change the softness/hardness of the repulsions and range of the attractive interactions. It can be expressed in a generalised LJ form as [152–155]

$$u(r) = \mathcal{C}\,\varepsilon\left[\left(\frac{\sigma}{r}\right)^{\lambda_r} - \left(\frac{\sigma}{r}\right)^{\lambda_a}\right], \tag{1}$$

where

$$\mathcal{C}(\lambda_a, \lambda_r) = \left(\frac{\lambda_r}{\lambda_r - \lambda_a}\right)\left(\frac{\lambda_r}{\lambda_a}\right)^{\frac{\lambda_a}{\lambda_r - \lambda_a}} \tag{2}$$

is defined such that the depth of the energetic potential well is $-\varepsilon$, the size of a spherical segment is σ, and the repulsive λ_r and attractive λ_a exponents characterise the form of the interaction.

The latest version of the SAFT equation of state (EoS) based on the Mie reference potential (SAFT-VR Mie) [156] and its reformulation as a group contribution approach (SAFT-γ Mie) [157] have recently been used to provide an efficient parameterisation of simple CG force fields for a variety of molecular fluids over a broad range of conditions, including carbon dioxide and other greenhouse gases, refrigerants, long *n*-alkanes, and aromatic compounds represented as homonuclear or heteronuclear models of tangentially bonded Mie segments [158–160]; the reader is directed to a recent review [161] for details of methodology and specific examples of the capabilities of the so-called SAFT-γ Mie CG force fields. The equation of state has also been parameterised in terms of a corresponding state correlation to allow the molecular parameters to be obtained from critical data [162], and the SAFT-γ Mie models are rapidly gaining popularity in the simulation of mixtures [163–165].

The analytical form of the EoS enables a rapid and efficient exploration of a wide parameter space enabling one to obtain a set of intermolecular potential parameters that provide an optimal description of the macroscopic experimental data. Using variable values of the exponents (as opposed to the LJ 12-6 form) has been shown to provide a significant improvement in the description of the vapour pressure and the second-derivative thermodynamic properties of real fluids, such as speed of sound, heat capacity, and compressibility [156–158,166]. The key advantage is that the parameters estimated from macroscopic fluid-phase equilibria data with the SAFT-γ top-down methodology can be used directly in microscopic molecular simulations.

2.2. *Molecular simulation details*

As mentioned earlier, we employ a simple Mie (generalised LJ) isotropic potential form to capture the effective intermolecular interactions between water molecules. The size and energy parameters of the models and the exponents that characterise the softness/hardness and range of the interactions are parameterised to reproduce target thermodynamic properties of water with the aid of the SAFT-VR/SAFT-γ Mie EoS [156,157]; one should note that in the case of the single-site models of water, the SAFT-VR and SAFT-γ approaches are equivalent. In our current study, the target properties are the vapour–liquid coexistence properties and interfacial tension. By employing the potential parameters obtained from the macroscopic properties with the EoS, the fluid-phase equilibria of our SAFT-γ Mie CG models of water can also be determined using direct MD simulation in the canonical ensemble, corresponding to a constant number of particles N, volume V, and temperature T [99]. The overall density of the system is chosen such that it lies inside the coexistence envelope according to the simulation procedure outlined in Ref. [167]. A system of $N = 8000$ water molecules is arranged in an orthorhombic simulation box with the usual periodic boundary conditions, where the box length L_z in the z direction is chosen such that it is approximately three times longer than that in the x and y directions. In this configuration, a liquid slab of water with two planar interfaces is formed in contact with low-density vapour. The simulations are carried out using the DL_POLY package, version 2.0 [168], and the equations of motion are solved using the leap-frog algorithm with a time step size of 10 fs. The system temperature is maintained constant using the Nosé–Hoover thermostat [169,170] with a coupling constant of 1.0 ps. The initial 300,000 time steps are discarded and the equilibrium properties are then sampled for an additional 300,000 time steps to obtain time averages of the properties of interest.

The densities of the coexisting liquid and vapour phases are determined from the density profiles at the corresponding temperature. The saturated-vapour pressure $P = P_v$ is calculated as the component of the pressure tensor normal to the interface. The enthalpy of vaporisation $\Delta H_v = \Delta U + P\Delta V$ (with U the internal energy) is found from the difference of the single-phase enthalpies evaluated for the vapour H_v and liquid H_l phases at the corresponding bulk densities.

The critical points are estimated from the vapour–liquid equilibrium MD simulation data using the standard scaling laws [171,172]. At each temperature, the corresponding liquid ρ_l and vapour ρ_v densities are related to the critical temperature T_c through

$$\rho_l - \rho_v = B_0|\tau|^{\beta_c}, \tag{3}$$

where $\tau = 1 - T/T_c$, B_0 is a system-dependent constant obtained by correlating the data, and $\beta_c = 0.325$ is the critical exponent fixed at its universal renormalisation-group value. The critical density ρ_c is estimated from the law of rectilinear diameters,

$$\frac{\rho_l + \rho_v}{2} = \rho_c + D_1|\tau|, \tag{4}$$

and the critical pressure is estimated from an extrapolation of the Clausius–Clapeyron relation to the critical temperature obtained from Equation (3)

$$\ln P = C_1 + \frac{C_2}{T}, \tag{5}$$

where D_1, C_1, and C_2 are correlation parameters.

We provide more details of the determination of the vapour–liquid interfacial tension by molecular simulation as this can prove to be problematic particularly in the correct treatment of the cut-off of the potential and long-range contributions [173,174]. A common method to calculate the interfacial tension is by means of a mechanical route, which requires the evaluation of forces [175] in order to obtain the

average Cartesian components $P_{\alpha\alpha}$ of the pressure tensor:

$$\gamma = \frac{1}{2}\int_0^{L_z}\left(P_{zz}(z) - \frac{P_{xx}(z)+P_{yy}(z)}{2}\right)\mathrm{d}z. \qquad (6)$$

The leading pre-factor of $\frac{1}{2}$ implies the presence of two interfaces in our particular case. For the geometry employed in our simulations, the saturated-vapour pressure is obtained from $P_v = P_{zz}$. Trokhymchuk and Alejandre [173] have shown that there can be issues with the determination of the pressure or the interfacial tension with the mechanical route for interactions with a (short) cut-off in the potential; the discontinuity in the potential at the cut-off leads to an impulse in the force which has to be taken into account explicitly in order to accurately determine the mechanical properties.

In order to ensure that the pressure and interfacial tension is reliably estimated for our CG models of water, we verify our calculations by employing an alternative thermodynamic route involving test-area (TA) perturbations [174]. In the TA approach, the interfacial tension is computed from infinitesimal virtual perturbations in the interfacial area (at constant overall volume), thereby inducing changes in the configurational energy and free energy of the system. The cut-off in the potential does not lead to computational issues for methods based on a calculation of the energy of the system. In the canonical ensemble, the surface tension of a planar interface can be obtained from the following thermodynamic definition:

$$\gamma = \left(\frac{\partial A}{\partial a}\right)_{NVT} = \lim_{\Delta a\to 0}\left(\frac{\Delta A}{\Delta a}\right)_{NVT}, \qquad (7)$$

where A is the Helmholtz free energy and a is the interfacial area. To perform a perturbation from the reference system 0 to a perturbed state 1, the box dimension in the x and y directions parallel to the interface are scaled such that $L_{x1} = L_{x0}\sqrt{1+\zeta}$ and $L_{y1} = L_{y0}\sqrt{1+\zeta}$, respectively, where ζ is a perturbation parameter corresponding to a change in the original interfacial area of $\Delta a_{0\to 1} = a_0\zeta = L_{x0}L_{y0}\zeta$. Since the volume of the system has to remain constant, the box dimension in the z direction normal to the interface is scaled as $L_{z1} = L_{z0}/(1+\zeta)$. The molecular coordinates are scaled such that the relative positions along each axis remain unchanged. The free energy difference $\Delta A_{0\to 1}$ between the reference and perturbed states can be estimated in terms of the Boltzmann factor of the corresponding change in the configurational energy according to the Zwanzig perturbation expression [174,176]:

$$\Delta A_{0\to 1} = -k_B T \ln\left\langle \exp\left(-\frac{\Delta U_{0\to 1}}{k_B T}\right)\right\rangle_0, \qquad (8)$$

where k_B is the Boltzmann constant and the angular brackets represent an average over the unperturbed reference system. The perturbations can involve either an increase ($0\to 1$) or a decrease ($0\to -1$) in the interfacial area, and the interfacial tension can then be obtained from a central difference scheme:

$$\gamma = \frac{A_{0\to 1} - A_{0\to -1}}{2\Delta a}. \qquad (9)$$

Three different values of the perturbation parameter ζ ($\zeta = 0.001$, 0.0005, and 0.0001) are employed in the procedure and the results are extrapolated to the limit of $\zeta = 0$. Adequate statistics are crucial for an accurate estimate of the interfacial tension by the TA method: the averages are computed over 1,000,000 time steps, for configurations every 100 time steps. The components of the pressure tensor can be computed from appropriate test-volume perturbations following a similar procedure; the reader is directed to Refs. [177–179] for details. While computationally more demanding, the results from the TA method do not suffer from errors due to an improper treatment of the potential cut-off. By comparing the interfacial tension obtained with the mechanical and TA approaches, one is able to make a critical assessment of the effect of the cut-off allowing for an appropriate choice to be made for a given model system. This is particularly important in the case of the softer, long-range potentials that are used to represent water.

3. Results

3.1. The effect of the cut-off of the potential on the thermodynamic properties

Before we discuss the development and parameterisation of the various models for water in detail, it is important to assess the effect of the cut-off of the potential on the vapour–liquid equilibria and interfacial tension. The cut-off radius R_c is usually introduced in molecular simulation to improve the computational efficiency by reducing the number of interactions to those between the neighbours within the cut-off distance. The truncation of the interactions is typically performed either by using spherically truncated (ST) or spherically truncated and shifted (STS) potential models. In MD simulations, this gives rise to a discontinuity in forces (which are the derivatives of the potential) at the cut-off distance. Depending on the molecular simulation software that is employed, the long-range corrections beyond the cut-off are treated in different approximate ways also giving rise to possible sources of errors. Trokhymchuk and Alejandre [173] have shown that the vapour–liquid surface tension of the LJ fluid increases by ~35% when the cut-off is increased from $R_c = 2.5\sigma$ to 4.4σ for the ST model and an even more significant ~ 60% for the STS model; the corresponding change in the density of the coexisting liquid phase is found to be ~10% and 15% for the

ST and STS models, respectively. Similar findings on the importance of a proper account of the cut-off radius have been reported by Wang *et al.* [180], who also employed a mechanical route to determine the interfacial tension. The tension was seen to have converged to that of the full LJ potential for a cut-off radius of about $R_c = 10\sigma$.

The expressions developed for the various contributions in the SAFT-VR/SAFT-γ perturbation theory account for the full range of the potential, i.e., an infinite cut-off. A suitable cut-off nevertheless has to be imposed in the calculation of the energies and forces within a finite molecular simulation cell. It is therefore essential to determine the value of R_c that is appropriate to reproduce the target thermodynamic properties of the full potential for our CG models of water (at least within a known and acceptable margin of error). As we will see in Section 3.2.2, the Mie (8-6) potential is particularly appropriate as an average representation of the interactions of water over the entire phase envelope. The Mie (8-6) potential is 'softer' and of a longer range than the LJ (12-6) potential, and as a consequence larger cut-offs are required in order for the thermodynamic properties to converge to those of the full potential model: the potential takes a value of $u(R_c = 5\sigma) = 5.8 \times 10^{-4}\varepsilon$ and $u(R_c = 10\sigma) = 9.4 \times 10^{-6}\varepsilon$. Despite these apparently small energies, the discrepancy in the resulting macroscopic properties is not negligible.

The vapour–liquid coexistence and interfacial properties of the ST Mie (8-6) system obtained by direct MD simulation for values of the cut-off ranging from $R_c \sim 5\sigma$ to 12σ are reported in Table 1. As a representative example, we start by examining the Mie (8-6) model of water developed in our current work to reproduce the vapour–liquid equilibria (CGW1-vle); a detailed description of the development of the model will be given in Section 3.3. The densities of the coexisting liquid and the vapour states and the vapour pressure of the CGW1-vle model are displayed in Figure 2 for a temperature of $T = 393$ K. It is apparent that a cut-off radius of at least $R_c = 30$ Å $\sim 10\sigma$ is required to reproduce the limiting value of the vapour pressure of the full potential model within the precision of the simulation technique.

Table 1. The vapour–liquid coexistence properties, including the saturated-liquid ρ_l and vapour ρ_v densities, and vapour pressure P_v for the CGW1-vle model of water obtained at a temperature of $T = 393$ K as a function of the cut-off radius R_c, obtained by MD simulations. The standard errors in the last significant figure, indicated in brackets, are determined from the standard deviation of the appropriate block averages [99].

R_c/Å	ρ_l/(kg m^{-3})	ρ_v/(kg m^{-3})	P_v/MPa
15	936(3)	1.34(13)	0.228(6)
20	944(2)	1.14(13)	0.211(6)
25	946(4)	1.10(13)	0.194(6)
30	949(3)	1.04(08)	0.191(4)
35	949(2)	1.02(08)	0.186(2)

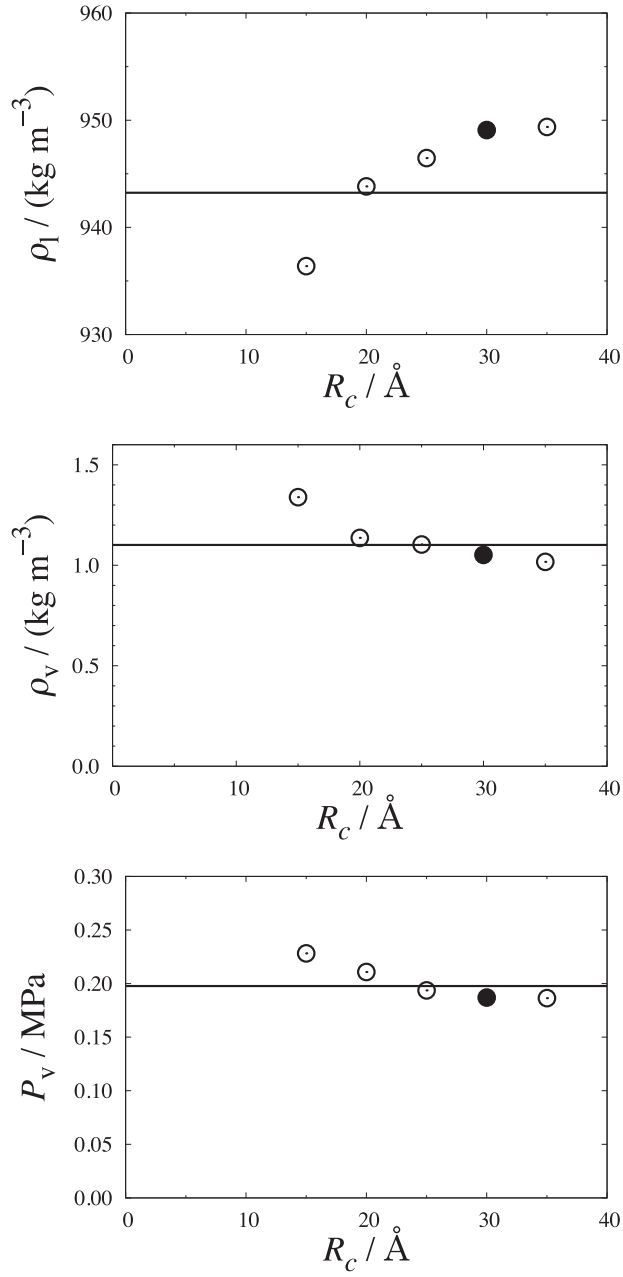

Figure 2. The vapour–liquid coexistence properties including the saturated-liquid ρ_l and vapour ρ_v densities, and vapour pressure P_v for our Mie (8-6) CGW1-vle model of water at a temperature of $T = 393$ K as a function of the cut-off radius R_c. The black lines denote the results obtained with the SAFT-γ Mie EoS [156,157]. The open circles are the corresponding MD simulation data and the filled circles denote the values for the cut-off radius of $R_c = 30$ Å chosen for the CGW1-vle model in our current study.

As will be described in detail in Section 3.4, we parameterise a second Mie (8-6) model (CGW1-ift) to reproduce the saturated-liquid density and the vapour–liquid interfacial tension of water. The interfacial tension of the ST CGW1-ift model is presented as a function of the cut-off radius in Figure 3. As for the vapour pressure, the tension is

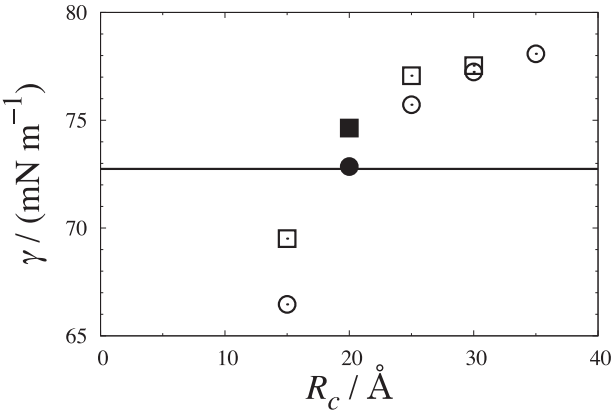

Figure 3. The vapour–liquid interfacial tension γ of our Mie (8-6) CGW1-ift model of water at a temperature of $T = 293$ K as a function of the cut-off radius R_c. The black line denotes the experimental surface tension of water. The circles are the MD simulation data obtained with the mechanical route, and the squares are the corresponding data obtained with the TA method; the filled symbols denote the values for the cut-off radius of $R_c = 20$ Å chosen for the CGW1-ift model in our current study.

found to converge to that of the full potential only for a large cut-off radius of $R_c \geq 30$ Å. The values of the vapour–liquid interfacial tension obtained with the mechanical and TA approaches are seen to be equivalent only for the large cut–off radii; the deviations from the full potential model found for the shorter cut-off radii are seen to be larger when estimated from the mechanical route. As a consequence, unless a very large cut-off radius is chosen, it is advisable to compute the surface tension by means of the TA method in order to minimise the effects of truncating the full potential. In a typical CG simulation, the cut-off is chosen to be between 9 and 15 Å (see, e.g., Refs. [105,107,112]), which is rather short in terms of reproducing the properties of the equivalent full potential. One should bear in mind that the cut-off radius is an important parameter of the model, and it is therefore crucial to consistently specify and use the same value to insure reproducibility of the results.

3.2. *Issues of transferability and representability of the force fields*

3.2.1. *Transferability*

It is well known [181] that CG of an intermolecular potential invariably leads to issues of representability and transferability of the structural and thermophysical properties. Problems with the transferability of the model occur if a force field developed to reproduce a given state point does not provide an adequate description at another state point, so that the potential has to be refined for the new state. Following a statistical mechanical description of the system, the Helmholtz free energy A of the CG representation can be obtained from a many-body PMF, which is directly related to the configurational integral:

$$\exp\left(-\frac{A}{k_B T}\right) = C \int_V \exp\left[-\left(\frac{U(\mathbf{r})}{k_B T}\right)\right] \mathrm{d}\mathbf{r} = C' \int_V \exp\left[-\left(\frac{U_{\mathrm{CG}}(\mathbf{R})}{k_B T}\right)\right] \mathrm{d}\mathbf{R}, \tag{10}$$

where $U(\mathbf{r})$ is the total intermolecular potential which is a function of the vector of configurational variables $\mathbf{r}$, and C and C' are specific constants that include kinetic contributions. The potential of mean force $U_{\mathrm{CG}}(\mathbf{R})$ is necessarily a function of the dimensionality of the system via the CG variables $\mathbf{R}$ and thermodynamic state, thereby depending on the temperature and density. For a highly polar fluid with directional interactions such as water, the many-body interactions play a significant role and cannot be effectively averaged in an equivalent fashion for all thermodynamic states [13,106]. The averaging of atomistic interactions into the effective interactions of a CG bead leads one to neglect some important microscopic physical detail. The Mie potential (like the specific LJ form) belongs to the group of spherically symmetrical (isotropic) force fields. The directional intermolecular forces which are responsible for the characteristic behaviour of water cannot be fully captured with a spherically symmetrical potential at different conditions, and a universal parameter set fails to reproduce the various target physical properties if a wide range of thermodynamic conditions are considered. For example, if we use the parameters for the Mie (8-6) potential of Section 3.3 parameterised to provide a good description of the saturated-liquid density and vapour pressure of water at ambient temperature (with $\sigma = 3.0089$ Å and $\varepsilon/k_B = 496.09$ K), the prediction of the vapour–liquid equilibria is very poor at higher temperatures: the critical temperature and liquid densities are markedly overestimated and the vapour pressure is underestimated (cf. Figure 4).

To overcome the problem of transferability of the intermolecular potential to other thermodynamic states, we consider temperature-dependent segment size and energy parameters. Our effective intermolecular potential can thus be considered as a free energy (or PMF). The re-parametrisation of a force field in this manner is typically a very inefficient procedure involving a number of iterative simulations at different conditions. The use of the algebraic SAFT-γ Mie EoS to obtain the underlying temperature dependence of the parameters greatly facilitates the process as a wide range of conditions can be considered at a fraction of the computational cost.

3.2.2. *Representability*

The issue of representability is associated with the fact that a given CG potential cannot be used to simultaneously represent all of the thermophysical properties of the system at

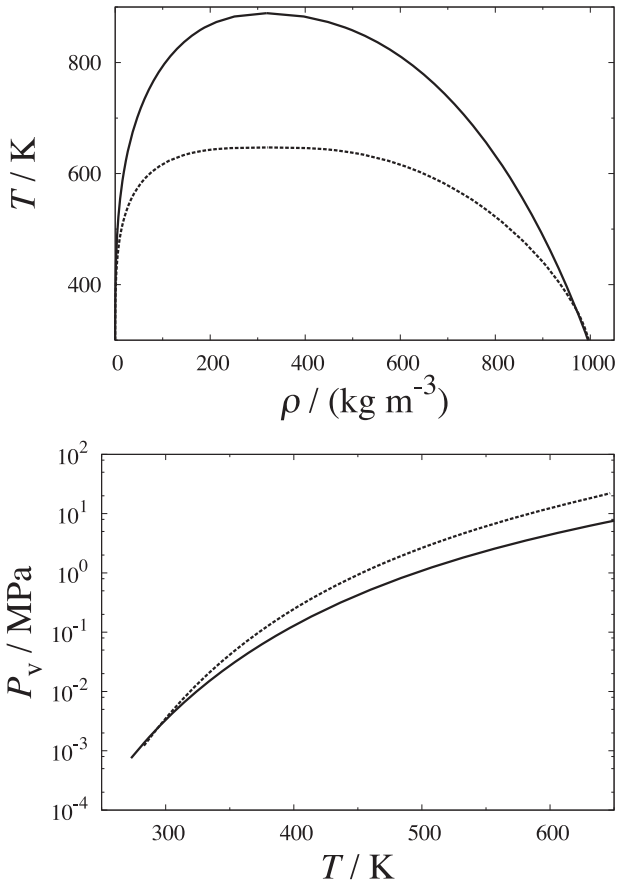

Figure 4. The coexisting vapour and liquid densities ρ and vapour pressure P_v of water, predicted with a universal parameter set, estimated from the corresponding properties at a temperature of $T = 298$ K: the model is a Mie (8-6) potential with $\sigma = 3.0089$ Å and $\varepsilon/k_B = 496.09$ K. The dashed curves denote the experimental values from NIST [185] and continuous curves are the predictions with the SAFT-γ Mie EoS [156,157] using the parameters obtained for the unique state point.

the same level of accuracy. As mentioned in the previous sections one can average out details of the atomistic interactions into an effective CG interaction based on the Mie form. The spherically symmetrical Mie potential is characterised by four parameters: the repulsive and attractive exponents, and the size and energy parameters. A central question is how many properties can be captured by tuning the four parameters to experimental data. Assuming that each parameter allows one to accurately represent a physical attribute, a given parameter would in principal determine a key target property.

In the context of force fields based on a Mie functional form, Ramrattan and co-workers [182,183] have undertaken a simple, yet very useful, analysis of the perturbation contributions at the heart of SAFT-VR and SAFT-γ Mie equations of state. According to the Barker and Henderson [184] high-temperature perturbation expansion, the residual Helmholtz free energy of a fluid of spherically symmetrical particles can be decomposed into a sum of the free energy associated with a reference hard-sphere system, a first-order perturbative contribution, and higher order terms. The first-order term corresponds to the so-called mean-attractive energy due to the attractive interactions. For a Mie fluid in the mean-field limit (corresponding to a uniform structure), the mean-attractive energy takes a simple van der Waals form, and a dimensionless van der Waals attractive constant α can be defined as [182,183]

$$\alpha(\lambda_a, \lambda_r) = \frac{1}{\varepsilon\sigma^3}\int_\sigma^\infty u(r) r^2 \mathrm{d}r = \mathcal{C}(\lambda_a, \lambda_r)\left[\left(\frac{1}{\lambda_a - 3}\right) - \left(\frac{1}{\lambda_r - 3}\right)\right], \tag{11}$$

with $\mathcal{C}(\lambda_a, \lambda_r)$ given in Equation (2). At the mean-field level, the mean-attractive energy of a Mie fluid is therefore a function of only three parameters, namely the size σ, energy ε, and van der Waals integrated energy $\alpha(\lambda_a, \lambda_r)$, the latter of which is itself a function of the attractive and repulsive exponents. As a consequence, two fluids with the same values of σ, ε, and α would exhibit the same thermodynamic properties at this level of approximation. Fluids with the same α would have a conformal intermolecular potential, implying that the exponents λ_a and λ_r are not independent and together provide only one additional degree of freedom. Due to this conformality, once the value of the energy parameter ε is fixed for a Mie potential with a prescribed pair of exponents, both the critical temperature T_c and the triple-point temperature T_t are then implicitly fixed. A simple linear correlation between the ratio of the critical and triple-point temperatures of the Mie system and α has been uncovered by Ramrattan and co-workers [182,183]: $T_c/T_t = 1.462\alpha + 0.603$.

For the common (12-6) combination of the LJ potential, the fluid range is characterised by $T_c/T_t \sim 1.9$, since for this fluid $T_c^* = k_B T_c/\varepsilon = 1.3$ and $T_t^* = k_B T_t/\varepsilon = 0.7$, corresponding to $\alpha = 0.89$. One could guarantee a sensible description of the critical point of water by matching the experimental critical temperature ($T_c = 647$ K) to the LJ model with $T_c^* = 1.3$, commensurate with the value of $\varepsilon/k_B = 498$ K. This choice then fixes the triple point of the LJ (12-6) model at $T_t = 348$ K (rather than the experimental value of 273 K), suggesting that any simulation at ambient temperature is prone to premature freezing. Conversely, the choice of the triple point as the target results in a cohesive interaction which is too weak compared to experiment and as a consequence to a fluid range which is unsatisfactorily small.

If one simply frees all of the parameters available for the Mie potential (i.e., the repulsive/attractive exponents, size, and energy parameters) as degrees of freedom to optimise the description of a maximum number of target thermodynamic properties of water with the SAFT-γ Mie EoS, the

model corresponding to a Mie (40-6) potential with $\sigma = 3.1065$ Å and $\varepsilon/k_B = 777$ K is found to provide a good representation of the critical temperature, saturated-liquid densities, and vaporisation enthalpies over a range of elevated temperatures. Unfortunately, the model with such a steep repulsive interaction and deep energetic well corresponds to a van der Waals attractive constant of $\alpha = 0.50$, implying that the system exhibits a very narrow liquid range and marked premature freezing with a triple point of $T_t \sim 464$ K.

A sensible choice of exponents for a Mie model of water is one that would allow one to match the experimental ratio of $T_c/T_t = 647/273 = 2.37$, which according to the correlation of Ramrattan and co-workers would correspond to a van der Waals parameter of $\alpha \sim 1.20$. There are of course an infinite number of pairs of exponents that satisfy this condition (cf. Equation (11)) [183]. For convenience, we retain the London form ($\lambda_a = 6$) of attractive contribution and are led to select the relatively soft Mie (8-6) potential, corresponding to a value of $\alpha = 1.26$; the latter is close to that expected for water from the simple scaling analysis, although the use of temperature-dependent size and energy parameters in the following sections complicates this type of direct analysis. The Mie (8-6) form is consistent with empirical observations made by He *et al.* [112], who assessed a number of models and recommended the use of the Mie (9-6) and (12-4) potentials for a one-to-one CG description of water, which would correspond to $\alpha = 1.13$ and $\alpha = 2.31$, respectively.

The form of the various intermolecular potentials discussed in the context of a CG representation of water are compared in Figure 5. The issue of premature freezing can be explained by assessing the well depth and the overall shape of the potential (particularly the steep repulsive region). The deepest well, and therefore the highest melting temperature, is expected for the Mie (40-6) model, followed by the MARTINI model. Our Mie (8-6) CGW1-vle model (parameterised to optimise the overall description of the fluid-phase equilibria of water, as described in Section 3.3) and the standard LJ (12-6) model have a comparably large well depth, and also give rise to freezing at ambient conditions; the Mie (8-6) potential is 'softer' and exhibits a more extensive fluid range than the LJ model. Our Mie (8-6) CGW1-ift model (parameterised to optimise the description of the saturated-liquid density and vapour–liquid interfacial tension, as described in Section 3.4) has a form which is very similar to the Mie (9-6) and (12-4) models suggested by He *et al.* [112], which is reassuring as the same properties of water are being targeted. The relatively soft nature of the Mie (8-6) potential and its shallow energetic well ensure that CGW1-ift model remains in a stable liquid state throughout the experimental liquid range. An entirely different form of potential is obtained with IBI technique based on the structure of the SPC water model [36]: unlike the models based on a CG potential characterised by a single well, the CG IBI potential is seen to exhibit multiple wells that account for the short-range hydrogen bonding and the long-range attractive interactions; the relatively shallow well means that the model will not suffer from premature freezing. (It is important to point out, however, that the aim of the IBI CG methodology is principally to reproduce the structural properties of the fluid; the thermodynamic properties are not considered explicitly with this approach and cannot be accurately reproduced [106]. A further disadvantage of the IBI approach is that the potential is not based on a closed algebraic form and instead has to be obtained with an iterative procedure at each state point, making it computationally demanding.)

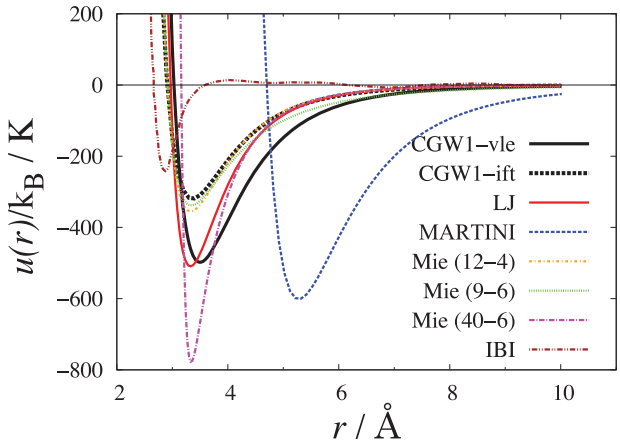

Figure 5. The various CG intermolecular potentials used to represent water at a temperature of $T = 298$ K: Mie (8-6) CGW1-vle model, developed with the SAFT-γ Mie EoS [156,157] to represent the saturated-liquid density and vapour pressure; Mie (8-6) CGW1-ift model, developed to represent the saturated-liquid density and vapour–liquid interfacial tension; the Mie (40-6) potential developed as a compromise to reproduce the saturated-liquid density, the vapour pressure, enthalpy of vaporisation, and vapour–liquid interfacial tension to a lower level of accuracy, but freezes at ambient conditions; the Mie (9-6) and (12-4) potentials proposed by He *et al.* [112] capture the saturated-liquid density and the vapour–liquid interfacial tension, but fail to describe the vapour pressure and the enthalpy of vaporisation; the MARTINI model [107], which corresponds to a simple LJ (12-6) potential form at the four-to-one molecules per bead level of CG, captures the liquid density but freezes prematurely; the LJ (12-6) potential at the one-to-one level of CG reproduces the liquid density but fails to describe the vapour pressure and enthalpy of vaporisation, and freezes at ambient conditions; the IBI model is obtained by mapping the structural properties of SPC model to a CG bead using IBI, without a consideration of the thermodynamic properties.

After having chosen the designated Mie (8-6) form of force field for our CG representation of water, the remaining size and energy parameters can be estimated by matching the appropriate target properties. A key quantity that is invariably used to parameterise the intermolecular potentials of fluid systems is the (saturated) liquid density. The accurate description of the density is closely linked to the value of the size parameter σ of the model. As the

representation of the liquid density is generally a prerequisite, this further reduces the available degrees of freedom, so that only the energy scale ε can be adjusted to capture the remaining properties (assuming of course that the form of the potential has already been fixed). In the next section, we will show that an attempt to match a given target property of water (e.g., the vapour pressure) with a Mie potential can lead to a significant deterioration in the prediction of another property (e.g., the vapour–liquid interfacial tension); this is perhaps not very surprising considering the highly simplified nature of the force field. The compromise of representing several properties simultaneously with a lower degree of accuracy is unfortunately found to be unsatisfactory. In order to address this issue, two alternative single-site Mie (8-6) CG models of water are developed in our current work with the aid of the SAFT-γ Mie EoS: the first model, CGW1-vle, is parameterised to faithfully reproduce the saturated-liquid density and the vapour pressure; the second model, CGW1-ift, to reproduce the saturated-liquid density and the vapour–liquid interfacial tension. As was mentioned in Section 3.2.1, temperature-dependent size and energy parameters are employed to ensure that the intermolecular potential is applicable for a broad range of thermodynamic states. We should note that this temperature dependence of the force field makes the assessment of the fluid range (cf. the simple analysis of Ramrattan and co-workers [182,183]) more complicated because the various Mie (8-6) models give rise to different critical and triple-point temperatures of the system (in real units).

3.3. *Mie (8-6) CGW1-vle model of water with the saturated-liquid density and vapour pressure as target properties*

The first Mie (8-6) model considered (CGW1-vle) is designed to provide an optimal description of the experimental saturated-liquid density and vapour pressure over the entire fluid phase range; the National Institute of Standards and Technology (NIST) database is used as a reliable and extensive source of experimental data [185]. To that effect, the size and energy parameters σ and ε are estimated with the SAFT-γ Mie EoS by minimising the difference between the experimental and theoretical values of these properties for a specified temperature. The parameter estimation procedure is undertaken for each state point, so that there is a parameter set for each temperature considered; the reader is directed to Refs. [158] and [159] for the specific form of objective function employed in such a methodology.

The temperature dependence obtained for the parameters is reported in Table 2 and plotted in Figure 6. Simple correlations for the size $\sigma(T)$ and energy $\varepsilon(T)$ parameters of our Mie (8-6) CGW1-vle model of water (for use with the relatively long cut-off of $R_c = 30$ Å, which essentially corresponds to the full potential) can then be developed as simple polynomial functions of the temperature:

$$\sigma/\text{Å} = 1.262 \times 10^{-9}(T/\text{K})^3 - 8.720 \times 10^{-8}(T/\text{K})^2 - 4.554 \times 10^{-4}(T/\text{K}) + 3.119 \quad (12)$$

and

$$(\varepsilon/k_B)/\text{K} = 1.105 \times 10^{-5}(T/\text{K})^2 - 0.3077(T/\text{K}) + 586.8. \quad (13)$$

Table 2. Temperature dependence of the Mie size $\sigma(T)$ and energy $\varepsilon(T)$ parameters for the Mie (8-6) CGW1-vle model of water at the one-to-one level of CG, designed to reproduce the saturated-liquid density and vapour pressure.

T/K	σ/Å	(ε/k_B)/K
343	3.0015	481.87
353	3.0014	478.82
363	3.0016	475.81
373	3.0021	472.83
393	3.0039	466.97
413	3.0065	461.20
433	3.0099	455.51
453	3.0141	449.85
463	3.0165	447.01
473	3.0192	444.21
493	3.0251	438.55
513	3.0321	432.82
533	3.0403	426.99
553	3.0503	420.98
563	3.0560	417.84
573	3.0627	414.68
593	3.0790	407.90
613	3.1028	400.21

It is apparent from Figure 6 that $\sigma(T)$ exhibits a minimum at a temperature of ~350 K, while $\varepsilon(T)$ is characterised by a near-linear temperature dependence.

The triple point of the Mie (8-6) model has been determined as $T_t^* = 0.71$ from the intersection of the bubble point curve for the saturated liquid with the solidification curve [182,183]. Using Equation (13), one finds that the state of the CGW1-vle model corresponding to the experimental triple point of water ($T_t = 273$ K) is at a reduced temperature of $T^* = k_B T_t/\varepsilon = 0.54$ which is below the triple-point value of 0.71 estimated for the Mie (8-6) force field; the CGW1-vle model therefore suffers from premature freezing with a triple point at ~343 K. The overestimate of the freezing point is unavoidable because of the high values of the energy parameters which are required for an accurate description of the vapour-pressure curve over the entire fluid range. The high values of the well depth ε can be attributed to the effective incorporation of the hydrogen bonding in our isotropic CG force field; the average attractive interaction is seen to decrease with increasing temperature which is consistent with expected breaking of hydrogen bonds. The physically meaningful temperature range

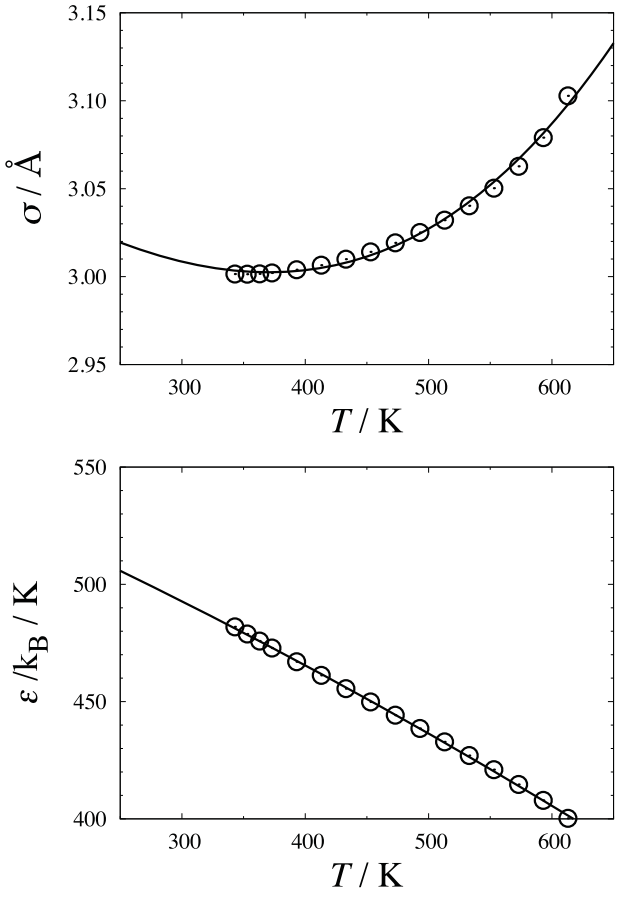

Figure 6. The temperature dependence of the size $\sigma(T)$ and energy $\varepsilon(T)$ parameters for the Mie (8-6) CGW1-vle model of water developed to reproduce the experimental saturated-liquid density and vapour pressure, as estimated with the SAFT-γ Mie EoS [156,157]. The continuous curves are the correlations of Equations (12) and (13).

for the model is therefore from the triple point of the model to the near-critical region. The Mie (8-6) CGW1-vle model is therefore parameterised for the description of the fluid-phase equilibria of water in the temperature range between 343 and 613 K. Extrapolating the parameter set beyond the given temperature range could lead to unphysical behaviour.

In order to retain a close link with the theory and faithfully represent the full potential, a relatively large value of $R_c = 30$ Å (corresponding to $R_c \sim 10\sigma$) is chosen for the cut-off radius to be used with CGW1-vle model in molecular simulation of the fluid-phase equilibria (cf. Figure 2). Overall, the accuracy of the prediction of the vapour–liquid equilibria with the SAFT-γ EoS [156,157] for the Mie (8-6) system compared to the MD simulation data obtained for the model with $R_c = 30$ Å (reported in Table 3) corresponds to a percentage absolute average deviation (% AAD) of 1% for the saturated-liquid density and 4% for the vapour pressure. It is apparent from Figure 7 that both the MD simulation and the EoS reproduce the experimental data very accurately with this model. As the CGW1-vle model is parameterised to specifically reproduce the saturated-liquid density and vapour pressure at each temperature along the vapour–liquid envelope, the prediction of other properties can unfortunately deviate from experimental values due to the aforementioned issues of representability. For instance, the enthalpy of vaporisation is underestimated by about 19% and the vapour–liquid interfacial tension is overpredicted by more than 100% at low temperatures (see Figure 8). A more significant drawback of the CGW1-vle model is, however, its high melting temperature which, as for the MARTINI force field of water, causes unphysical freezing at ambient conditions.

Notwithstanding these deficiencies, our Mie (8-6) CGW1-vle model is suitable for the description of fluid-phase equilibria of water, including aqueous mixtures at elevated temperatures and pressures. The one-to-one mapping can be used to account for the behaviour of water molecules in the vapour phase in a reasonably realistic manner, in contrast to CG models of water involving more than one water molecule per bead, which imply an unphysical clustering in the vapour phase. The excellent performance of the CGW1-vle model for binary aqueous systems is illustrated for the vapour–liquid and liquid–liquid phase

Table 3. The vapour–liquid coexistence properties, including the saturated-liquid ρ_l and vapour ρ_v densities, vapour pressure P_v, vapour–liquid interfacial tension γ, and enthalpy of vaporisation ΔH_v for the Mie (8-6) CGW1-vle model of water at different temperatures T obtained by MD simulations using a cut-off radius of $R_c = 30$ Å. The standard errors in the last significant figure, indicated in brackets, are determined from the standard deviation of the appropriate block averages [99].

T/K	ρ_l/(kg m^{-3})	ρ_v/(kg m^{-3})	P_v/MPa	γ/(mN m^{-1})	ΔH_v/(kJ mol^{-1})
343	995(3)	0.17(4)	0.026(4)	159.0(4)	33.99(4)
363	978(3)	0.38(8)	0.066(5)	147.3(3)	33.05(7)
393	949(3)	1.0(1)	0.191(4)	131.0(3)	33.07(1)
433	907(3)	3.0(2)	0.579(5)	110.0(1)	31.24(1)
463	872(2)	5.9(3)	1.190(6)	93.7(1)	29.76(1)
493	833(3)	10.3(3)	2.17(3)	78.4(2)	28.17(1)
533	775(3)	20.1(7)	4.39(3)	58.4(4)	25.75(1)
563	724(2)	32.0(8)	6.96(4)	44.5(2)	23.57(1)
593	662(3)	49.0(9)	10.47(3)	30.3(3)	20.96(1)

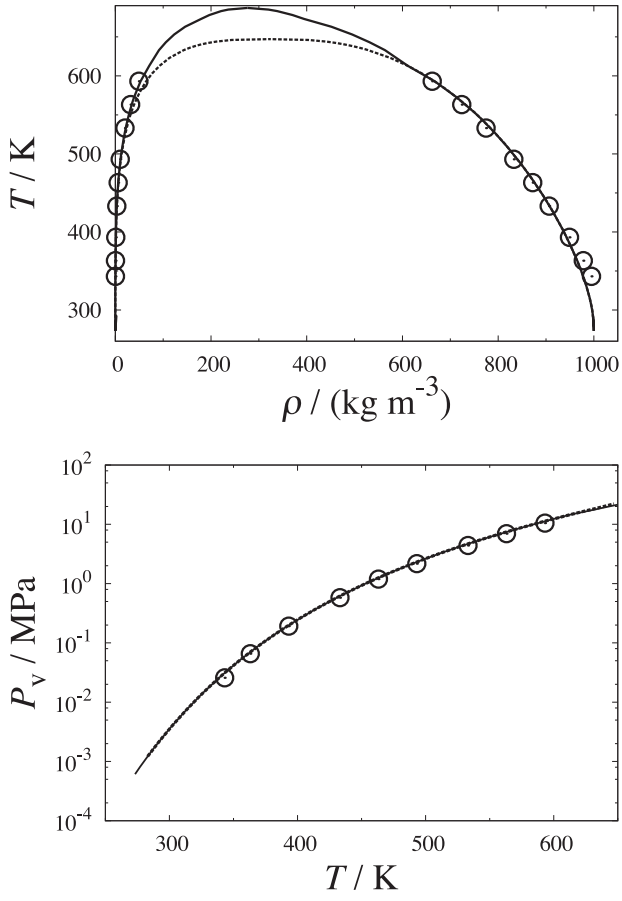

Figure 7. The coexisting vapour and liquid densities ρ and vapour pressure P_v of water as represented with the Mie (8-6) CGW1-vle model. The dashed curves denote the correlated experimental values from NIST [185], the continuous curves are the description with the SAFT-γ Mie EoS [156,157] (indistinguishable from the experimental values of the vapour pressure at this resolution), and the symbols are the corresponding data obtained by MD simulations.

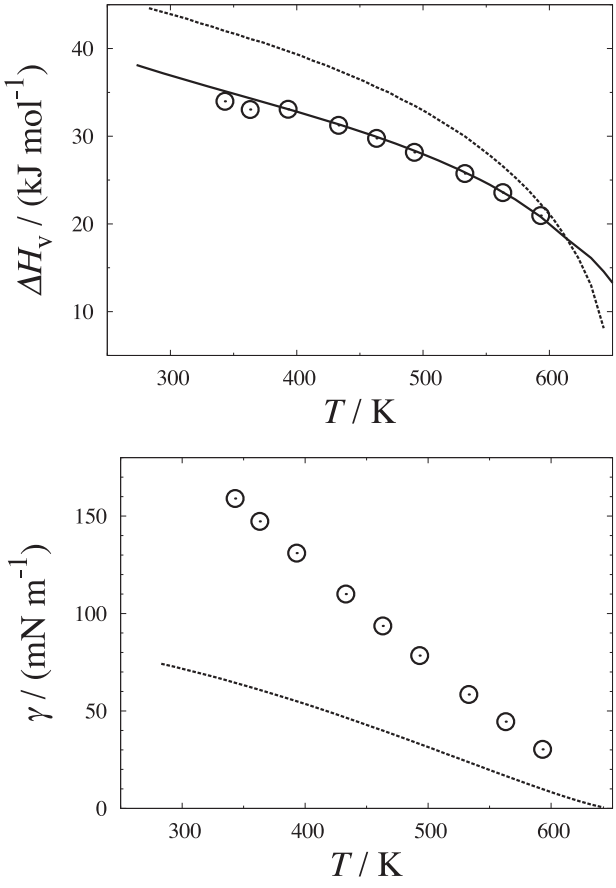

Figure 8. The enthalpy of vaporisation ΔH_v and vapour–liquid interfacial tension γ of water as represented with the Mie (8-6) CGW1-vle model. The dashed curves denote the correlated experimental values from NIST [185], the continuous curve is the description with the SAFT-γ Mie EoS [156,157], and the symbols are the corresponding data obtained by MD simulations.

equilibria of mixtures with carbon dioxide and *n*-alkanes in Ref. [186].

3.4. Mie (8-6) CGW1-ift model of water with the saturated-liquid density and vapour–liquid interfacial tension as target properties

In studies of biological systems, most of the relevant phenomena, such as the phase morphologies of aqueous solutions of amphiphilic molecules or the configurations of macromolecular structures, take place in the liquid phase. An accurate description of the interfacial tension is crucial in order to best capture the physical properties of these systems, as the phase morphology of the microphase separated domains is very sensitive to details of the interfacial properties [105]. We therefore propose an alternative parameterisation with model CGW1-ift focusing of the accurate reproduction of the liquid density and surface tension, again at the one-to-one level of course graining.

The exponent pair characterising our Mie CGW1-ift model of water is kept as (8-6) for the sake of consistency, and the size $\sigma(T)$ and energy $\varepsilon(T)$ parameters are estimated directly from the molecular simulation data for the saturated-liquid density and the vapour–liquid interfacial tension at each temperature; the prediction of the latter is not directly accessible from the SAFT-VR EoS (unless a suitable treatment of the inhomogeneous properties of the system is made [187–189]).

The parameterisation is undertaken to match the interfacial tension (as determined with the mechanical route), using the cut-off radius of $R_c = 20$ Å as a compromise between an accurate representation of the full potential (corresponding to $R_c > 30$ Å) and the computational effort associated with longer ranged interactions; the corresponding simulation data for $R_c = 20$ Å is reported in Table 5. The values of vapour–liquid interfacial tension obtained with the pressure–tensor mechanical and TA thermodynamic routes

Table 4 Temperature dependence of the Mie size $\sigma(T)$ and energy $\varepsilon(T)$ parameters for the Mie (8-6) CGW1-ift of water at the one-to-one level of CG, designed to reproduce the saturated-liquid density and vapour–liquid interfacial tension.

T/K	σ/ Å	(ε/k_B)/K
293	2.9055	304.28
298	2.9016	305.21
313	2.8938	309.01
343	2.8811	318.84
373	2.8737	326.85
393	2.8721	332.18
433	2.8673	340.25
463	2.8660	345.43
493	2.8666	350.25

for $R_c = 20$ Å are indicated in Figure 3 (cf. the discussion in Section 3.1); for this cut-off radius, a small difference of $\sim$2 mN m^{-1} is observed in the values of the tension obtained with the two approaches at ambient conditions.

The temperature-dependent parameter set for $\sigma(T)$ and $\varepsilon(T)$ of the Mie (8-6) CGW1-ift model of water is given in Table 4 and plotted in Figure 9. Correlations for the size and energy parameters of the CGW1-ift model (for use with a cut-off of $R_c = 20$ Å) can also be developed as simple polynomial functions of the temperature:

$$\sigma/\text{Å} = -6.455 \times 10^{-9}(T/\text{K})^3 + 9.100 \times 10^{-6}(T/\text{K})^2 - 4.291 \times 10^{-3}(T/\text{K}) + 3.543 \quad (14)$$

and

$$(\varepsilon/k_B)/\text{K} = -4.806 \times 10^{-4}(T/\text{K})^2 + 0.6107(T/\text{K}) + 165.9. \quad (15)$$

The values of the parameters obtained at ambient conditions are in a similar range to those of the one-to-one CG Mie (12-4) and (9-6) models of water developed by He *et al.* [112], which were also parameterised to reproduce the liquid density and surface tension. As a consequence of the comparatively low values of the well depth ε for these models, the system remains in the liquid state over the whole experimental temperature range of the fluid. The state point of the CGW1-ift model system corresponding to a temperature of 273 K is above the experimental triple

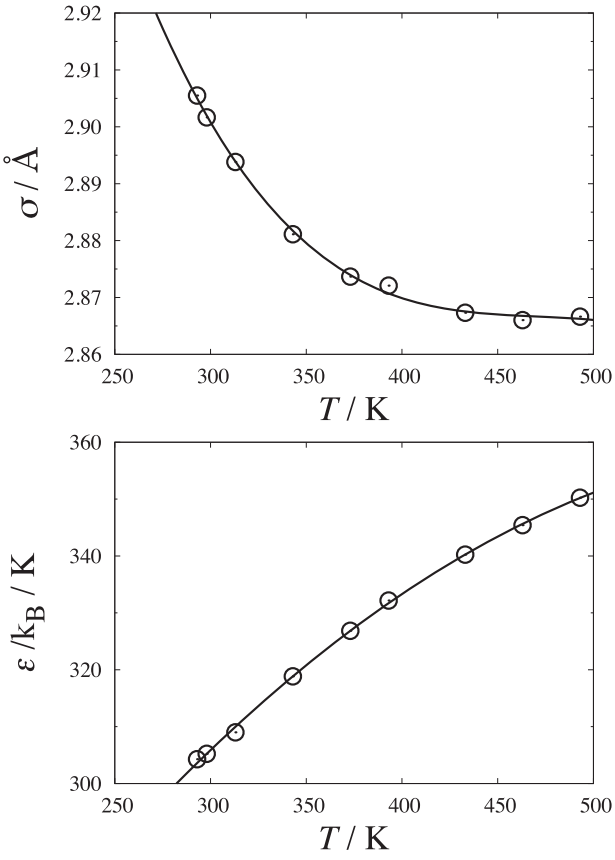

Figure 9. Temperature dependence of the size $\sigma(T)$ and energy $\varepsilon(T)$ parameters of the Mie (8-6) CGW1-ift model of water developed to reproduce the experimental saturated-liquid density and vapour–liquid interfacial tension, as estimated from the corresponding simulation data for the model. The continuous curves are the correlations of Equations (14) and (15).

Table 5. The vapour–liquid coexistence properties including the saturated-liquid ρ_l and vapour ρ_v densities, vapour pressure P_v, vapour–liquid interfacial tension γ, and enthalpy of vaporisation ΔH_v for the Mie (8-6) CGW1-ift model of water at different temperatures T obtained by MD simulations using a cut-off radius of $R_c = 20$ Å. The standard errors in the last significant figure, indicated in brackets, are determined from the standard deviation of the appropriate block averages [99].

T/K	ρ_l/(kg m^{-3})	ρ_v/(kg m^{-3})	P_v/MPa	γ/(mN m^{-1})	ΔH_v/(kJ mol^{-1})
293	999(4)	4.0 (3)	0.52 (1)	72.6 (1)	20.6 (1)
298	998(4)	4.3 (3)	0.58 (1)	71.5 (3)	20.6 (1)
313	992(4)	5.9 (4)	0.81 (1)	68.4 (3)	20.6 (1)
343	979(4)	9.2 (4)	1.38 (1)	64.3 (2)	21.4 (1)
373	960(3)	14.1 (5)	2.25 (3)	59.1 (2)	20.7 (1)
393	943(4)	17.9 (6)	2.96 (2)	54.9 (1)	20.6 (1)
433	907(4)	29.0 (9)	5.01 (4)	46.3 (3)	20.0 (1)
463	875(3)	40.0 (8)	7.05 (3)	39.0 (4)	19.4 (1)
493	840(5)	54.5 (9)	9.73 (4)	32.6 (2)	18.5 (1)

point; the triple point of the model now corresponds to the relatively low temperature of $T_t \sim 193$ K.

The saturated-liquid densities and the surface tensions of the model obtained by direct MD simulation of a liquid slab in coexistence with vapour are in excellent agreement with the experimental data over the entire fluid temperature range as can be seen from Figure 10. As discussed earlier, there can be problems of representability with CG models of this type for properties not employed in the parameterisation: at low temperatures, the enthalpy of vaporisation and vapour pressure predicted with the CGW1-ift model deviates significantly from the experimental data (see Figure 11).

Our Mie (8-6) CGW1-ift model is therefore ideally suited for studies of the condensed liquid state and interfacial properties of aqueous solutions of, e.g., surfactants, biological systems, and macromolecules in general. The CGW1-ift model is being used as a model of the solvent for aqueous solutions of non-ionic surfactants to accurately describe the micellar and lamellar structures formed in

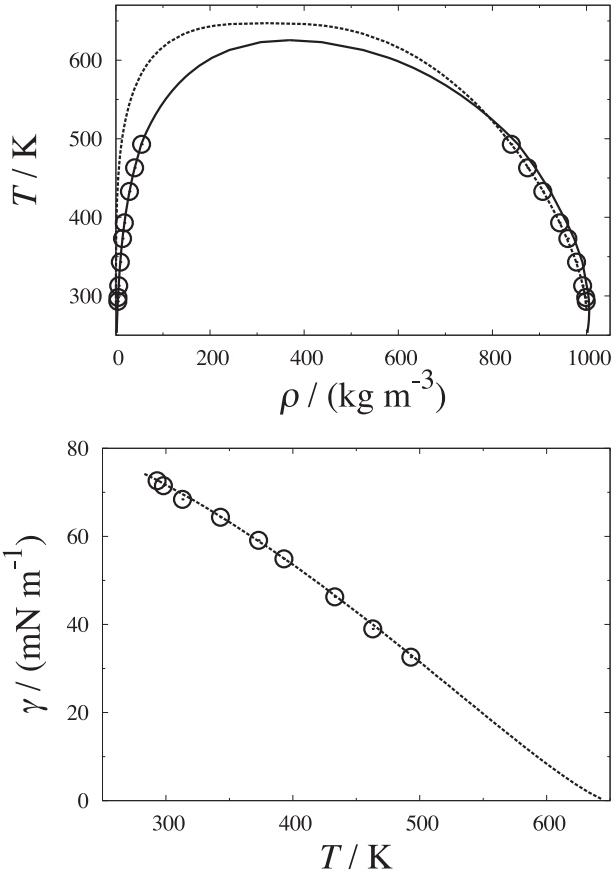

Figure 10. The coexistence vapour and liquid densities ρ and vapour–liquid interfacial tension γ of water as predicted with the Mie (8-6) CGW1-ift model. The dashed curves denote the correlated experimental values from NIST [185], the continuous curve is the prediction with the SAFT-γ Mie EoS [156,157], and the symbols are the corresponding data obtained for the system by MD simulations.

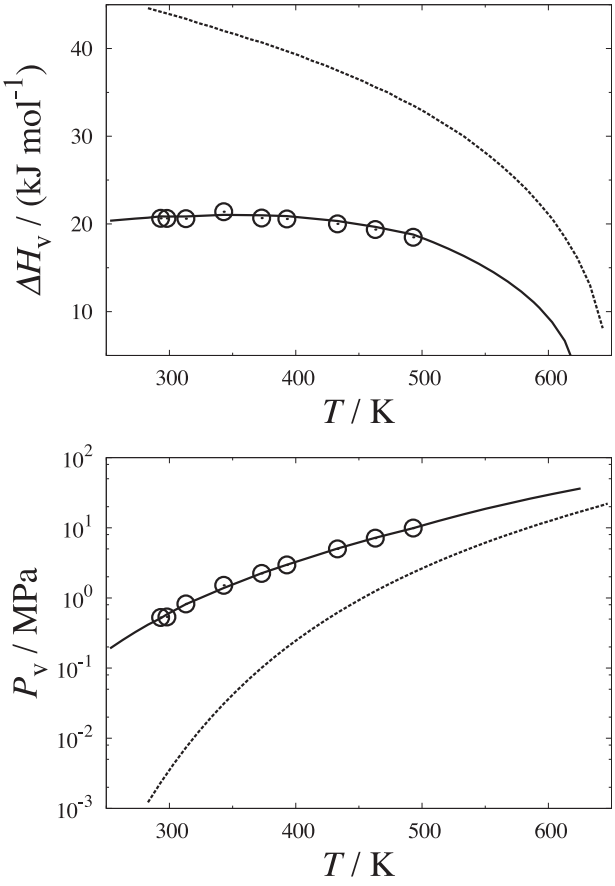

Figure 11. The enthalpy of vaporisation ΔH_v and vapour pressure P_v of water as predicted with the Mie (8-6) CGW1-ift model. The dashed curves denote the correlated experimental values from NIST [185], the continuous curves are the predictions with the SAFT-γ Mie EoS [156,157], and the symbols are the corresponding data obtained for the system by MD simulations.

such systems [190]. A preliminary version of our CGW1-vle model has also been used to represent the interfacial properties of aqueous mixtures of carbon dioxide [191] and methane [192]; it is important to point out that the temperature-dependent size and energy parameters used in these recent studies do not correspond precisely to our final optimal description captured by Equations (14) and (15).

3.5. *Different levels of coarse graining of water and the CGW2-bio model*

In this section, we explore different levels of CG for the Mie (8-6) model of water, ranging from one to four molecules per bead. In previous work, He *et al.* [112] observed that at the higher levels of CG, the water models parameterised to reproduce the liquid density and surface tension give rise to unphysical crystalline states at ambient conditions. As mentioned earlier, the triple point for the Mie (8-6) model is at $T_t^* = 0.71$. The size and energy parameter can be obtained from the representation of the liquid density and surface tension as explained in the previous section (for the

Table 6. Parameters for the Mie (8-6) models of water at different molecule-to-bead levels of CG developed to reproduce the saturated-liquid density and vapour–liquid interfacial tension at a temperature of $T = 298$ K, and the corresponding normal melting temperatures T_m. A cut-off radius of $R_c = 20$ Å is prescribed for all of the models.

CG level	1	2	3	4
σ/Å	2.9016	3.7467	4.3310	4.8295
(ε/k_B)/K	305	400	481	573
T_m/K	193	282	341	407

particular case of the one-to-one mapping). The parameters obtained in this manner at different levels of CG are reported in Table 6 together with the corresponding normal melting points. It is apparent that the marked overestimation of the melting point is a direct consequence of the CG of more than two water molecules per bead (for the Mie (8-6) model at least).

The level of CG should not therefore be chosen higher than two water molecules per bead in order to avoid unphysical freezing at ambient temperatures. From this simple analysis, the best choice for large-scale simulations of aqueous surfactants or macromolecular biological systems that retains and accurate description of the fluid would correspond to two-to-one mapping. In this regard, we develop a Mie (8-6) model of water at the two-to-one level of CG (CGW2-bio model), which is parameterised to reproduce the saturated-liquid density and surface tension at ambient conditions. The cut-off radius is fixed to $R_c = 20$ Å, as for the CGW1-ift model described in the previous section. A unique set of temperature-independent size $\sigma = 3.7467$ Å and energy $\varepsilon/k_B = 400$ K parameters is employed for temperatures between 293 and 313 K, unavoidably leading to small deviations in liquid densities and surface tensions at the limits of the said temperature range (see Table 7). The model is particularly useful for large-scale simulation of aqueous surfactants or biomolecular systems where the low solute concentrations require very large numbers of water molecules, with the sole purpose of acting as the medium. A further advantage is the decrease in the vapour pressure associated with an increase in the level of CG, so that the description of the vapour pressure with our two-to-one CGW2-bio model is improved by one order of magnitude compared to that with the CG models based on a one-to-one mapping.

Our Mie (8-6) CGW2-bio model has already been successfully implemented to elucidate the mechanism of superspreading [193], a challenging computational task due to the large time and length scales required to faithfully describe the spreading of drops on surfaces [194]. An interesting consequence of this aggressive CG and the relative long range of the resulting force field is that finite-size effects are more noticeable. As an example, simulations of the contact angle of a nano-droplet of this model on a surface require up to half a million CG beads to reach a stable size-independent value [195]. The increase in the computational effort for the large system size is, however, more than compensated by the significant efficiency gained by employing the CG force field.

Table 7. The Mie (8-6) CGW2-bio model corresponding to a two-to-one molecule-to-bead mapping is parameterised to reproduce the saturated-liquid density ρ_l and vapour–liquid interfacial tension γ at ambient conditions. The size and energy parameters for the model are constant over the temperature range considered: $\sigma = 3.7467$ Å and $\varepsilon/k_B = 400$ K. The values of the vapour–liquid interfacial tension γ, the saturated liquid density ρ_l, and vapour pressure P_v obtained by MD simulation are compared with the corresponding experimental values [185].

T/K	293	298	303	313
	MD simulation			
γ/(mN m^{-1})	73.4	71.9	71.1	69.2
ρ_l/(kg m^{-3})	1004	999	995	986
P_v/kPa	21.7	30.3	34.7	47.9
	Experiment			
γ/(mN m^{-1})	72.8	72.0	71.2	69.6
ρ_l/(kg m^{-3})	998	997	996	992
P_v/kPa	2.3	3.1	4.2	7.3

3.6. *Comparison of the Mie (8-6) CG models of water with existing models*

As a final assessment of the various force fields for water, we compare the performance of our Mie (8-6) CG models with some of the popular atomistic and other CG models. The molecular parameters for the various models are summarised in Table 8. The computational performance of our Mie (8-6) CGW1-ift one-to-one model in typical MD simulations is compared to that for the atomistic SPC model [36–38] in Figure 12. As is evident from the figure, the

Table 8. Parameter sets for the atomistic and CG water models, including the size σ and energy ε parameters, the repulsive λ_r and attractive λ_a exponents, the cut-off radius R_c of the Mie potentials, and the proton charges q_H of the atomistic models.

Water models	σ/Å	(ε/k_B)/K	λ_r	λ_a	R_c/Å	q_H/e
		CG models				
CGW1-vle ($T = 298$ K)	3.0089	496.09	8	6	30	
CGW1-vle ($T = 450$ K)	3.0114	450.57	8	6	30	
CGW1-ift ($T = 298$ K)	2.9016	305.21	8	6	20	
CGW1-ift ($T = 450$ K)	2.8666	343.39	8	6	20	
CGW2-bio	3.7467	400.00	8	6	20	
He *et al.* [112]	2.9080	354.77	9	6	15	
MARTINI [107]	4.7	601.36	12	6	12	
		Atomistic models				
TIP3P	3.1506	76.54	12	6		0.417
TIP4P	3.1540	78.02	12	6		0.52
TIP4P/2005	3.1589	93.20	12	6		0.5564
SPC	3.1656	78.20	12	6		0.41
SPC/E	3.1656	78.20	12	6		0.423

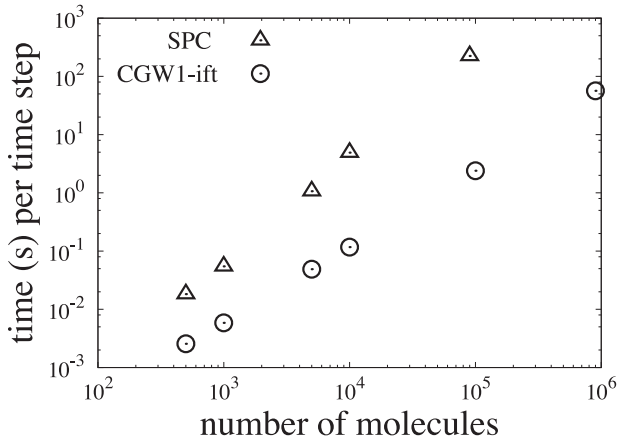

Figure 12. Comparison of the CPU time per time step in typical MD simulations of water as a function of number of molecules for our Mie (8-6) CGW1-ift model and the atomistic SPC model [36–38]. The state point corresponds to the saturated liquid at a temperature of $T = 298$ K. The simulations are performed in the canonical *NVT* ensemble on eight CPU 3 GHz processors employing the DL_POLY 2.0 package [168].

representation of the water molecule as a single CG bead with no explicit electrostatics leads to compelling savings in computational time. The expected gain in computational efficiency is between one and two order of magnitude in terms of the system size [for a fixed central processor unit (CPU) time per time step], and about two orders of magnitude in the simulation speed-up for a fixed system size. This performance makes our CG model attractive for calculations of large systems over long times. The benefits of employing the CGW2-bio model at the two-to-one level of course graining is an additional gain in efficiency by factor of four.

A comparison of the accuracy in representing the thermodynamic properties of water at room temperature ($T = 298$ K) and at a higher temperature of $T = 450$ K with the various CG and atomistic models is summarised in Table 9: our Mie (8-6) CGW1-vle, CGW1-ift, and CGW2-bio models are examined along with the MARTINI (12-6) [107] and the (9-6) [112] CG models, and the popular atomistic force fields, including popular incarnations of TIP [41] and SPC [36–38] families. One should recall that the temperature of $T = 298$ K is below the triple point of the CGW1-vle model; this state represents a metastable fluid which we assess by means of the SAFT-γ Mie EoS [156,157]. The same applies to the MARTINI CG force-field of water, where the calculation of properties of the pure liquid at ambient temperature is only possible following the modification proposed by Chiu *et al.* [113]. Representative thermophysical properties, including the saturated-liquid density ρ_l, vapour pressure P_v, enthalpy of vaporisation ΔH_v, vapour–liquid interfacial tension γ, isobaric heat capacity c_P, isobaric thermal expansivity α_P, isothermal compressibility κ, self-diffusion coefficient D_s, and second-virial B_2 coefficient, are assessed in Table 9. When not available from the literature, the properties of the various Mie systems are calculated as averages by performing MD simulations as described in Section 2.2. The corresponding ambient melting points and the extent of the vapour–liquid phase envelope quantified in terms of the ratio of the normal melting point and critical temperatures are also compared. For the CG models, the melting points are obtained from the analysis described in Section 3.2.2; the normal boiling points are estimated from the Clausius–Clapeyron relation, [Equation (5)]; the critical points are obtained from the scaling laws, [Equations (3) and (4)]; the second-derivative thermodynamic properties are predicted using the SAFT-γ Mie EoS; and the second-virial coefficients of isotropic particles are calculated from the statistical mechanical definition involving the radial integral of the Mayer function [171]. The properties for the atomistic TIP and SPC models are taken from the corresponding literature [7,8,42,46,54,55,118,196,197].

The performance of the atomistic models of water is generally better than for the CG models, as one would expect with any force field at a higher level of resolution. It is important to recognise, however, that none of these atomistic models can be used to accurately reproduce all of the properties simultaneously despite the more significant computational requirements. Considering their simple nature, the description with our CG models is still very satisfactory for the target properties under consideration. At high temperature, our CG models represent the liquid density of water more accurately than any of non-polarisable atomistic models considered here. The vapour pressure and second-virial coefficient determined with the CGW1-vle model are also in closer agreement to the experimental values than those corresponding to the other models; this is not surprising as the CGW1-vle model is specifically designed to capture the properties of the liquid and the vapour phase simultaneously. It is well known that rigid non-polarisable atomistic models, which are typically parameterised to reproduce the properties of the liquid phase, cannot be used to reproduce properties of the vapour phase reliably [7,198].

As an additional comparison, the self-diffusion coefficients of the saturated liquid determined from the mean-square displacement [99] in MD simulations of our CG models and the various atomistic models of water are represented as a function of the inverse temperature in Figure 13. One would expect the self-diffusion coefficient to be overestimated relative to the experimental value for a CG description; the CG beads have a higher mobility because the water molecules are not slowed down by the re-orientation of the hydrogen atoms and the formation/break-up of hydrogen bonds [110]. The Mie (8-6) CGW1-ift model indeed conforms with this behaviour: the diffusion coefficients obtained at low temperatures are markedly overestimated and become comparable with the experimental values for water only in the high-temperature limit. By contrast, the self-diffusion coefficient determined

Table 9. Comparison of the thermophysical properties for water at 298 K or at 300 K* and 1 atm for the CG and atomistic models: the values are given for the ratio of the melting and critical temperatures T_m/T_c, the normal melting T_m, normal boiling T_b, and critical T_c temperatures, the saturated-liquid density ρ_l, the vapour pressure P_v, the vapour–liquid tension γ, the enthalpy of vaporisation ΔH_v, the isobaric heat capacity c_P, the isobaric thermal expansivity α_P, the isothermal compressibility κ_T, the self-diffusion coefficient D_s, and the second-virial coefficient B_2. The values without citations are estimated in our current work, either via MD simulation or with the SAFT-γ Mie EoS [156,157]. The experimental data is taken from NIST [185].

	Coarse-grained models					Atomistic models					
	CGW1 -vle	CGW1 -ift	CGW2 -bio	MARTINI [107]	Mie (9-6) [112]	TIP3P	TIP4P	TIP4P /2005	SPC	SPC/E	Expt.
T_m/T_c	0.514	0.293	0.407	0.532	0.451	0.25 [7]	0.394 [7]	0.394 [7]	0.321 [7]	0.337 [7]	0.422
T_m/K	343	193	282	417	253	146 [7]	232 [7]	252 [7]	190 [7]	215 [7]	273
T_b/K	373	235	335	368	258	367 [7]	364 [55]	401 [55]	368 [54]	398 [54]	373
T_c/K	667	659	694	797	570	578 [7]	588 [7]	640 [7]	592 [7]	638 [7]	647
					$T = 298$ K (or $T = 300$ K*)						
ρ_l/(kg m^{-3})	997	998	999	1005 [113]	1000	1002 [42]	988 [8]	993 [8]	972 [118]	994 [118]	997
P_v/kPa	3.1	583	30	7.9	417	5.2* [7]	–	0.78* [55]	4.6 [54]	0.98 [54]	3.1
γ/(mN m^{-1})	179	72	72	32 [113]	72	52.3* [7]	59* [8]	69* [8]	53 [118]	64* [8]	72
ΔH_v/(kJ mol^{-1})	37	21	29	30.2 [113]	23	42 [8]	45 [8]	50 [8]	–	49 [8]	44
c_P/(J K^{-1} mol^{-1})	49	50	48	58	51	78 [8]	84 [8]	88 [8]	64 [118]	87 [8]	75
α_P/(10^{-4} K^{-1})	4.2	11	6	5.6	9.8	9.2 [7]	4.4 [7]	2.8 [7]	7.4 [197]	5 [197]	2.6
κ_T/(GPa^{-1})	0.14	0.42	0.43	0.9 [113]	0.35	0.64 [7]	0.59 [7]	0.46 [7]	0.53 [197]	0.47 [197]	0.45
D_s/(10^{-9}m^2 s^{-1})	1.7	7.4	3.8	1.6 [113]	5.8	5.5 [7]	3.2 [7]	2.1 [7]	4.2 [118]	2.4 [118]	2.3
					$T = 450$ K						
ρ_l/(kg m^{-3})	887	888	864	887	793	790 [7]	823 [8]	879 [8]		860 [8]	890
P_v/kPa	849	6016	1272	721	9144	1195 [7]	1330 [8]	446 [8]		580 [8]	932
γ/(mN m^{-1})	101	43	40	19	23	24.7 [7]	27.5 [8]	41.8 [8]		36.7 [8]	43
B_2/(cm^3 mol^{-1})	−150	−77	−108	−127	−72	−476 [8]	−396 [8]	−635 [8]		−653 [8]	−238

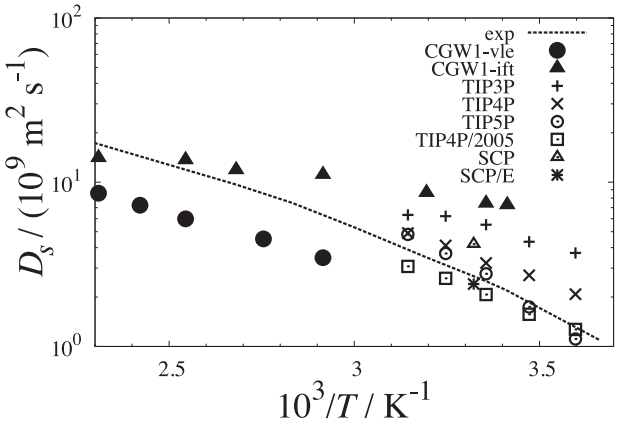

Figure 13. Self-diffusion coefficient D_s of the saturated liquid as a function of the inverse temperature $1/T$. The dashed curve denotes correlated experimental data [7], and the symbols represent the corresponding values obtained for the various atomistic and CG models by MD simulations; the data for our Mie (8-6) CG models are denoted as filled symbols, and the corresponding values for the TIP and SPC atomistic models are taken from Ref. [7].

with the Mie (8-6) CGW1-vle model is underestimated relative to experiment; this can be attributed to the large values of the energetic well of the potential which is a consequence of the use of the vapour pressure as the target property.

4. Conclusions

We have introduced CG single-site force fields for water, which are developed for targeted thermodynamic properties with the aid of the SAFT-γ Mie EoS based on the Mie (generalised LJ) interaction potential [156,157]. The use of the algebraic EoS as a top-down CG platform to develop SAFT-γ Mie force fields [161] has been applied to broad classes of molecular fluids, including carbon dioxide [158], greenhouse gases [159], hydrocarbons [159,199], aromatics [160], and amphiphilic molecules [190]. In the case of the water molecule examined in our current work, we have parameterised simple isotropic single-site models based on a relatively soft Mie (8-6) intermolecular potential. One finds, however, that a fixed form of intermolecular potential cannot be used to accurately represent all of the thermodynamic properties of water simultaneously. Two different one-to-one molecule-to-bead CG Mie (8-6) models of water are developed to target specific thermodynamic properties: the CGW1-vle model is designed to provide an optimal description of the saturated-liquid density and the vapour pressure, as a force field for use in the simulation of high-temperature high-pressure fluid-phase equilibria of aqueous systems; the CGW1-ift model is designed to accurately capture the saturated-liquid density and vapour–liquid interfacial tension, and is therefore particularly suited for the prediction of the interfacial

properties of aqueous solutions in the dense liquid phase. Since the effective CG interactions vary markedly with the temperature and density, temperature-dependent size and energy parameters are introduced to provide a reliable representation of the thermophysical properties over a broad range of conditions. The performance of our CG models compares favourably with the commonly used CG and atomistic models with at least two generic properties accurately reproduced over the entire temperature range of the liquid (which is not generally true of existing models). The CGW1-vle model is developed at the one-to-one mapping level of CG and can be used to represent the vapour–liquid equilibrium of aqueous mixtures reliably, while force fields that result from more aggressive CG lead to unphysical clustering and are unsuitable to represent the vapour phase.

To a certain extent, all CG models suffer from issues of representability for the different types of thermodynamic properties and transferability when extended to different thermodynamic states; this is particularly true for water and aqueous systems. The advantage of our methodology is that it is straightforward to implement an alternative parameterisation if different thermodynamic properties or conditions are of interest. The level of CG mapping can also be tuned for specific applications. In this vein, we have also proposed a Mie (8-6) model of water at the two-to-one molecule-to-bead level (CGW2-bio), parameterised to reproduce the liquid density and vapour–liquid interfacial tension at ambient conditions. The CGW2-bio model is therefore designed for use in large-scale simulations of aqueous solutions of amphiphiles, lipid membranes, proteins, and other challenging biomolecular systems. The relative simplicity of the CG representation means that fewer intermolecular parameters between the different species in mixtures have to be specified. Furthermore, the unlike interactions between the various chemical moieties in the system can also be estimated reliably with the aid of the SAFT-γ Mie EoS from appropriate macroscopic experimental data for the given mixture [161].

Acknowledgements

We are indebted to Carlos Vega for his invaluable insight and for helping us to navigate the extensive literature on the simulation of aqueous systems. Thanks are also due to Nina Ramrattan and Amparo Galindo for very useful discussions on the positions of the melting boundaries for the Mie models and for providing us access to their work prior to publication. Olga Lobanova is very grateful to Imperial College London for an Excellence Award in support of her PhD studies.

Disclosure statement

No potential conflict of interest was reported by the authors.

Funding

The work carried out in the Molecular Systems Engineering Group is financially supported by the Engineering and Physical Sciences Research Council (EPSRC) of the UK [grant number GR/T17595], [grant number GR/N35991], [grant number EP/E016340], [grant number EP/J014958]; the Joint Research Equipment Initiative (JREI) [grant number GR/M94426]; and the Royal Society-Wolfson Foundation refurbishment scheme [grant number RSWF/SUC11/RND3/EEP].

References

[1] A. Ben-Naim, *Molecular Theory of Water and Aqueous Solutions, Part 1: Understanding water* (World Scientific, Singapore, 2009).
[2] F. Paesani and G.A. Voth, J. Phys. Chem. B **113**, 5702 (2009).
[3] M.D. Baer, C.J. Mundy, M.J. McGrath, I.F.W. Kuo, J.I. Siepmann, and D.J. Tobias, J. Chem. Phys. **135**, 124712 (2011).
[4] B. Santra, J. Klimes, A. Tkatchenko, D. Alfe, B. Slater, A. Michaelides, R. Car, and M. Scheffler, J. Chem. Phys. **139**, 154702 (2013).
[5] B. Guillot and Y. Guissani, J. Chem. Phys. **114**, 6720 (2001).
[6] B. Guillot, J. Mol. Liq. **101**, 219 (2002).
[7] C. Vega, J.L.F. Abascal, M.M. Conde, and J.L. Aragones, Faraday Discuss. **141**, 251(2009).
[8] C. Vega and J.L.F. Abascal, Phys. Chem. Chem. Phys. **13**, 19663 (2011).
[9] I. Shvab and R.J. Sadus, J. Chem. Phys. **139**, 194505 (2013).
[10] O. Demerdash, E.H. Yap, and T. Head-Gordon, Annu. Rev. Phys. Chem. **65**, 149 (2014).
[11] S.O. Nielsen, C.F. Lopez, G. Srinivas, and M.L. Klein, J. Phys.: Condens. Matter **16**, R481(2004).
[12] K.A. Dill, T.M. Truskett, V. Vlachy, and B. Hribar-Lee, Annu. Rev. Biophys. Biomol. Struct. **34**, 173 (2005).
[13] A. Chaimovich and M.S. Shell, Phys. Chem. Chem. Phys. **11**, 1901 (2009).
[14] K.R. Hadley and C. McCabe, Mol. Simul. **38**, 671 (2012).
[15] C. Knight and G.A. Voth, Mol. Phys. **110**, 935 (2012).
[16] A. Striolo, Adsorption Sci. Technol. **29**, 211 (2011).
[17] S.L. Meadley and C.A. Angell, Water and its relatives: the stable, supercooled and particularly the stretched, regimes (open lectures) in *Proceedings of the International School of Physics "Enrico Fermi" Course CLXXXVII* (2014). Varenna, Italy.
[18] O. Matsuoka, E. Clementi, and M. Yoshimine, J. Chem. Phys. **64**, 1351 (1976).
[19] R. Car and M. Parrinello, Phys. Rev. Lett. **55**, 2471 (1985).
[20] S. Yoo, X.C. Zeng, and S.S. Xantheas, J. Chem. Phys. **130**, 221102 (2009).
[21] E. Miliordos, E. Apra, and S.S. Xantheas, J. Chem. Phys. **139**, 114302 (2013).
[22] M.J. McGrath, J.I. Siepmann, I.F.W. Kuo, and C.J. Mundy, Mol. Phys. **104**, 3619 (2006).
[23] M.J. McGrath, J.I. Siepmann, I.F.W. Kuo, C.J. Mundy, J. VandeVondele, J. Hutter, F. Mohamed, and M. Krack, J. Phys. Chem. A **110**, 640 (2006).
[24] D. Alfe, A.P. Bartok, G. Csanyi, and M.J. Gillan, J. Chem. Phys. **141**, 014104 (2014).
[25] E.E. Santiso and K.E. Gubbins, Mol. Simul. **30**, 699 (2004).
[26] P.G. Karamertzanis, P. Raiteri, and A. Galindo, J. Chem. Theory Comput. **6**, 1590 (2010).
[27] J.D. Bernal and R.H. Fowler, J. Chem. Phys. **1**, 515 (1933).

[28] J.S. Rowlinson, Trans. Faraday Soc. **45**, 974 (1949).
[29] J.S. Rowlinson, Trans. Faraday Soc. **47**, 120 (1951).
[30] J.A. Pople, Proc. Royal Soc. A **205**, 163 (1951).
[31] N. Bjerrum, Kgl. Danske Videnskab. Selskab, Math.-fys. Medd., **27**, 1 (1951).
[32] J.A. Barker and R.O. Watts, Chem. Phys. Lett. **3**, 144 (1969).
[33] A. Ben-Naim and F.H. Stillinger, Aspects of the Statistical-Mechanical Theory of Water in *Water and Aqueous Solutions: Structure, Thermodynamic and Transport Processes*, edited by R.A. Horne (Wiley, New York, 1972).
[34] F.H. Stillinger and A. Rahman, J. Chem. Phys. **60**, 1545 (1974).
[35] F.H. Stillinger, Theory and Molecular Models for Water in *Advances in Chemical Physics: Non-simple Liquids*, edited by I. Prigogine and S. Rice, (Wiley, New York, 1975).
[36] H. Berendsen, J. Postma, W. van Gunsteren, and J. Hermans, Interaction Models for Water in Relation to Protein Hydration in *Intermolecular Forces*, edited by B. Pullman (Reidel, Dordrecht, 1981), Vol. 14, pp. 331–342.
[37] J. Hermans, H.J.C. Berendsen, W.F. Van Gunsteren, and J.P.M. Postma, Biopolymers **23**, 1513 (1984).
[38] H.J.C. Berendsen, J.R. Grigera, and T.P. Straatsma, J. Phys. Chem. **91**, 6269 (1987).
[39] W.L. Jorgensen, J. Am. Chem. Soc. **103**, 335 (1981).
[40] W.L. Jorgensen, J. Chem. Phys. **77**, 4156 (1982).
[41] W.L. Jorgensen, J. Chandrasekhar, J.D. Madura, R.W. Impey, and M.L. Klein, J. Chem. Phys. **79**, 926(1983).
[42] M.W. Mahoney and W.L. Jorgensen, J. Chem. Phys. **112**, 8910 (2000).
[43] S.W. Rick, J. Chem. Phys. **120**, 6085 (2004).
[44] H.W. Horn, W.C. Swope, J.W. Pitera, J.D. Madura, T.J. Dick, G.L. Hura, and T. Head-Gordon, J. Chem. Phys. **120**, 9665 (2004).
[45] J.L.F. Abascal, E. Sanz, R.G. Fernandez, and C. Vega, J. Chem. Phys. **122**, 234511 (2005).
[46] J.L.F. Abascal and C. Vega, J. Chem. Phys. **123**, 234505 (2005).
[47] Y.L. Huang, T. Merker, M. Heilig, H. Hasse, and J. Vrabec, Ind. Eng. Chem. Res. **51**, 7428(2012).
[48] J.R. Errington and A.Z. Panagiotopoulos, J. Chem. Phys. **109**, 1093 (1998).
[49] E. Sanz, C. Vega, J.L.F. Abascal, and L.G. MacDowell, J. Chem. Phys. **121**, 1165 (2004).
[50] E. Sanz, C. Vega, J.L.F. Abascal, and L.G. MacDowell, Phys. Rev. Lett. **92**, 255701 (2004).
[51] P.G. Kusalik and I.M. Svishchev, Science **265**, 1219(1994).
[52] P. Jedlovszky and J. Richardi, J. Chem. Phys. **110**, 8019 (1999).
[53] P.T. Kiss and A. Baranyai, J. Chem. Phys. **134**, 054106 (2011).
[54] G.C. Boulougouris, I.G. Economou, and D.N. Theodorou, J. Phys. Chem. B **102**, 1029 (1998).
[55] C. Vega, J.L.F. Abascal, and I. Nezbeda, J. Chem. Phys. **125**, 034503 (2006).
[56] A. Baranyai, A. Bartok, and A.A. Chialvo, On the Performance of Simple Planar Models of Water in *The Vapor and the Ice Phases in Physics and Chemistry of Ice*, edited by F. Wilhelms and W.F. Kuhs (Royal Society of Chemistry, Cambridge, 2007).
[57] F.H. Stillinger and C.W. David, J. Chem. Phys. **69**, 1473 (1978).
[58] P. Barnes, J.L. Finney, J.D. Nicholas, and J.E. Quinn, Nature **282**, 459 (1979).
[59] A.A. Chialvo and P.T. Cummings, J. Chem. Phys. **105**, 8274 (1996).
[60] P. Paricaud, M. Predota, A.A. Chialvo, and P.T. Cummings, J. Chem. Phys. **122**, 244511 (2005).
[61] P. Kiss, M. Darvas, A. Baranyai, and P. Jedlovszky, J. Chem. Phys. **136**, 114706 (2012).
[62] P.T. Kiss, P. Bertsyk, and A. Baranyai, J. Chem. Phys. **137**, 194102 (2012).
[63] P.T. Kiss and A. Baranyai, J. Chem. Phys. **138**, 204507 (2013).
[64] L.P. Wang, T. Head-Gordon, J.W. Ponder, P. Ren, J.D. Chodera, P.K. Eastman, T.J. Martinez, and V.S. Pande, J. Phys. Chem. B **117**, 9956 (2013).
[65] S.W. Rick, S.J. Stuart, and B.J. Berne, J. Chem. Phys. **101**, 6141 (1994).
[66] B. Chen, J.H. Xing, and J.I. Siepmann, J. Phys. Chem. B **104**, 2391 (2000).
[67] M. Sprik and M.L. Klein, J. Chem. Phys. **89**, 7556 (1988).
[68] I.M. Svishchev, P.G. Kusalik, J. Wang, and R.J. Boyd, J. Chem. Phys. **105**, 4742 (1996).
[69] P. Ren and J.W. Ponder, J. Phys. Chem. B **107**, 5933 (2003).
[70] P. Ren and J.W. Ponder, J. Phys. Chem. B **108**, 13427 (2004).
[71] J.W. Ponder, C.J. Wu, P. Ren, V.S. Pande, J.D. Chodera, M.J. Schnieders, I. Haque, D.L. Mobley, D.S. Lambrecht, R.A. DiStasio, M. Head-Gordon, G.N.I. Clark, M.E. Johnson, and T. Head-Gordon, J. Phys. Chem. B **114**, 2549 (2010).
[72] P. J. van Maaren and D. van der Spoel, J. Phys. Chem. B **105**, 2618 (2001).
[73] P. Bopp, G. Jancso, and K. Heinzinger, Chem. Phys. Lett. **98**, 129(1983).
[74] Y.J. Wu, H.L. Tepper, and G.A. Voth, J. Chem. Phys. **124**, 024503 (2006).
[75] G. Raabe and R.J. Sadus, J. Chem. Phys. **134**, 234501 (2011).
[76] P.T. Kiss and A. Baranyai, J. Chem. Phys. **140**, 154505 (2014).
[77] A. Ben-Naim, J. Chem. Phys. **54**, 3682 (1971).
[78] K.A.T. Silverstein, A.D.J. Haymet, and K.A. Dill, J. Am. Chem. Soc. **120**, 3166 (1998).
[79] T.M. Truskett, P.G. Debenedetti, S. Sastry, and S. Torquato, J. Chem. Phys. **111**, 2647 (1999).
[80] P.H. Poole, F. Sciortino, T. Grande, H.E. Stanley, and C.A. Angell, Phys. Rev. Lett. **73**, 1632 (1994).
[81] E.A. Jagla, Phys. Rev. E **58**, 1478 (1998).
[82] E.A. Jagla, J. Chem. Phys. **111**, 8980 (1999).
[83] G. Franzese, G. Malescio, A. Skibinsky, S.V. Buldyrev, and H.E. Stanley, Nature **409**, 692 (2001).
[84] Z.Y. Yan, S.V. Buldyrev, N. Giovambattista, and H.E. Stanley, Phys. Rev. Lett. **95**, 130604(2005).
[85] A.B. de Oliveira, P.A. Netz, T. Colla, and M.C. Barbosa, J. Chem. Phys. **125**, 124503 (2006).
[86] A.B. de Oliveira, P.A. Netz, T. Colla, and M.C. Barbosa, J. Chem. Phys. **124**, 084505 (2006).
[87] G. Franzese, J. Mol. Liq. **136**, 267 (2007).
[88] S.V. Buldyrev, P. Kumar, P.G. Debenedetti, P.J. Rossky, and H.E. Stanley, Proc. Natl. Acad. Sci. USA **104**, 20177 (2007).
[89] A.B. de Oliveira, G. Franzese, P.A. Netz, and M.C. Barbosa, J. Chem. Phys. **128**, 064901 (2008).
[90] A. Perera, A. Rispe, L. Zoranic, R. Mazighi, and F. Sokolic, Mol. Phys. **107**, 1349 (2009).
[91] P. Vilaseca and G. Franzese, J. Chem. Phys. **133**, 084507 (2010).
[92] E. Salcedo, A.B. de Oliveira, N.M. Barraz, C. Chakravarty, and M.C. Barbosa, J. Chem. Phys. **135**, 044517 (2011).

[93] P. Vilaseca and G. Franzese, J. Non-Cryst. Solids **357**, 419 (2011).
[94] T. Urbic, Condens. Matter Phys. **16**, 43605 (2013).
[95] M. Hus and T. Urbic, J. Chem. Phys. **139**, 114504 (2013).
[96] M. Hus and T. Urbic, J. Chem. Phys. **140**, 144904 (2014).
[97] I. Nezbeda, J. Mol. Liq. **73–74**, 317 (1997).
[98] E.A. Müller and K.E. Gubbins, Ind. Eng. Chem. Res. **34**, 3662 (1995).
[99] M.P. Allen and D.J. Tildesley, *Computer Simulation of Liquids* (Oxford University Press, Oxford, 1987).
[100] T. Head-Gordon and F.H. Stillinger, J. Chem. Phys. **98**, 3313 (1993).
[101] J.C. Shelley, M.Y. Shelley, R.C. Reeder, S. Bandyopadhyay, and M.L. Klein, J. Phys. Chem. B **105**, 4464 (2001).
[102] V. Molinero and W.A. Goddard, J. Phys. Chem. B **108**, 1414 (2004).
[103] S.J. Marrink, A.H. de Vries, and A.E. Mark, J. Phys. Chem. B **108**, 750 (2004).
[104] S. Izvekov and G.A. Voth, J. Phys. Chem. B **109**, 2469 (2005).
[105] W. Shinoda, R. Devane, and M.L. Klein, Mol. Simul. **33**, 27(2007).
[106] M.E. Johnson, T. Head-Gordon, and A.A. Louis, J. Chem. Phys. **126**, 144509 (2007).
[107] S.J. Marrink, H.J. Risselada, S. Yefimov, D.P. Tieleman, and A.H. de Vries, J. Phys. Chem. B **111**, 7812 (2007).
[108] S. Izvekov, J.M.J. Swanson, and G.A. Voth, J. Phys. Chem. B **112**, 4711 (2008).
[109] H. Wang, C. Junghans, and K. Kremer, Eur. Phys. J. E **28**, 221(2009).
[110] V. Molinero and E.B. Moore, J. Phys. Chem. B **113**, 4008 (2009).
[111] M. Winger, D. Trzesniak, R. Baron, and W.F. van Gunsteren, Phys. Chem. Chem. Phys. **11**, 1934(2009).
[112] X.B. He, W. Shinoda, R. DeVane, and M.L. Klein, Mol. Phys. **108**, 2007 (2010).
[113] S.W. Chiu, H.L. Scott, and E. Jakobsson, J. Chem. Theory Comput. **6**, 851 (2010).
[114] M.U. Hammer, T.H. Anderson, A. Chaimovich, M.S. Shell, and J. Israelachvili, Faraday Discuss. **146**, 299 (2010).
[115] K.R. Hadley and C. McCabe, J. Phys. Chem. B **114**, 4590 (2010).
[116] Z. Wu, Q.A. Cui, and A. Yethiraj, J. Phys. Chem. B **114**, 10524 (2010).
[117] L. Darre, M.R. Machado, P.D. Dans, F.E. Herrera, and S. Pantano, J. Chem. Theory Comput. **6**, 3793(2010).
[118] S. Riniker and W.F. Gunsteren, J. Chem. Phys. **134**, 084110 (2011).
[119] W.F.D. Bennett and D.P. Tieleman, J. Chem. Theory Comput. **7**, 2981 (2011).
[120] L. Gao and W. Fang, J. Chem. Phys. **135**, 184101 (2011).
[121] B. van Hoof, A.J. Markvoort, R.A. van Santen, and P.A.J. Hilbers, J. Phys. Chem. B **115**, 10001 (2011).
[122] S.Y. Mashayak and N.R. Aluru, J. Chem. Phys. **137**, 214707 (2012).
[123] H.C. Gonzalez, L. Darre, and S. Pantano, J. Phys. Chem. B **117**, 14438 (2013).
[124] F. Zipoli, T. Laino, S. Stolz, E. Martin, C. Winkelmann, and A. Curioni, J. Chem. Phys. **139**, 094501 (2013).
[125] J.C. Fogarty, S.W. Chiu, P. Kirby, E. Jakobsson, and S.A. Pandit, J. Phys. Chem. B **118**, 1603 (2014).
[126] M. Orsi, Mol. Phys. **112**, 1566 (2014).
[127] L.C. Jacobson, R.M. Kirby, and V. Molinero, J. Phys. Chem. B **118**, 8190 (2014).
[128] S.J. Marrink, A.H. de Vries, T.A. Harroun, J. Katsaras, and S.R. Wassall, J. Am. Chem. Soc. **130**, 10 (2008).
[129] W.F.D. Bennett, J.L. MacCallum, M.J. Hinner, S.J. Marrink, and D.P. Tieleman, J. Am. Chem. Soc. **131**, 12714 (2009).
[130] T. Vuorela, A. Catte, P.S. Niemela, A. Hall, M.T. Hyvonen, S.J. Marrink, M. Karttunen, and I. Vattulainen, Plos Comput. Biol. **6**, e1000964 (2010).
[131] H. Lee, A.H. de Vries, S.J. Marrink, and R.W. Pastor, J. Phys. Chem. B **113**, 13186 (2009).
[132] H. Lee and R.W. Pastor, J. Phys. Chem. B **115**, 7830 (2011).
[133] A.V. Sangwai and R. Sureshkumar, Langmuir **27**, 6628(2011).
[134] M. Velinova, D. Sengupta, A.V. Tadjer, and S.J. Marrink, Langmuir **27**, 14071 (2011).
[135] C.A. Lopez, A.J. Rzepiela, A.H. de Vries, L. Dijkhuizen, P.H. Hunenberger, and S.J. Marrink, J. Chem. Theory Comput. **5**, 3195 (2009).
[136] P.J. Bond and M.S.P. Sansom, J. Am. Chem. Soc. **128**, 2697 (2006).
[137] A.Y. Shih, A. Arkhipov, P.L. Freddolino, and K. Schulten, J. Phys. Chem. B **110**, 3674 (2006).
[138] X. Periole, T. Huber, S.J. Marrink, and T.P. Sakmar, J. Am. Chem. Soc. **129**, 10126 (2007).
[139] L. Monticelli, S.K. Kandasamy, X. Periole, R.G. Larson, D.P. Tieleman, and S.J. Marrink, J. Chem. Theory Comput. **4**, 819(2008).
[140] M. Seo, S. Rauscher, R. Pomes, and D.P. Tieleman, J. Chem. Theory Comput. **8**, 1774(2012).
[141] W. Shinoda, R. DeVane, and M.L. Klein, Soft Matter **4**, 2454 (2008).
[142] M.L. Klein and W. Shinoda, Science **321**, 798(2008).
[143] W. Shinoda, R. DeVane, and M.L. Klein, Soft Matter **7**, 6178 (2011).
[144] D.N. LeBard, B.G. Levine, R. DeVane, W. Shinoda, and M.L. Klein, Chem. Phys. Lett. **522**, 38 (2012).
[145] B.L. Bhargava and M.L. Klein, Mol. Phys. **107**, 393 (2009).
[146] G. Srinivas and M.L. Klein, Nanotechnology **18**, 205703 (2007).
[147] W. Shinoda, R. DeVane, and M.L. Klein, J. Phys. Chem. B **114**, 6836 (2010).
[148] R. DeVane, A. Jusufi, W. Shinoda, C.C. Chiu, S.O. Nielsen, P.B. Moore, and M.L. Klein, J. Phys. Chem. B **114**, 16364 (2010).
[149] R. DeVane, W. Shinoda, P.B. Moore, and M.L. Klein, J. Chem. Theory Comput. **5**, 2115(2009).
[150] D.A. Pantano and M.L. Klein, J. Phys. Chem. B **113**, 13715 (2009).
[151] G. Mie, Ann. Phys. (Berlin) **316**, 657 (1903).
[152] E.A. Grüneisen, Ann. Phys. (Berlin) **344**, 257 (1912).
[153] J.E. Jones, Proc. R. Soc. A **106**, 441 (1924).
[154] J.E. Jones, Proc. R. Soc. A **106**, 463 (1924).
[155] J.E. Lennard-Jones, Proc. Phys. Soc. **43**, 461 (1931).
[156] T. Lafitte, A. Apostolakou, C. Avendaño, A. Galindo, C.S. Adjiman, E.A. Müller, and G. Jackson, J. Chem. Phys. **139**, 154504 (2013).
[157] V. Papaioannou, T. Lafitte, C. Avendaño, C.S. Adjiman, G. Jackson, E.A. Müller, and A. Galindo, J. Chem. Phys. **140**, 054107 (2014).
[158] C. Avendaño, T. Lafitte, A. Galindo, C.S. Adjiman, G. Jackson, and E.A. Müller, J. Phys. Chem. B **115**, 11154 (2011).
[159] C. Avendaño, T. Lafitte, C.S. Adjiman, A. Galindo, E.A. Müller, and G. Jackson, J. Phys. Chem. B **117**, 2717 (2013).

[160] T. Lafitte, C. Avendaño, V. Papaioannou, A. Galindo, C.S. Adjiman, G. Jackson, and E.A. Müller, Mol. Phys. **110**, 1189 (2012).
[161] E.A. Müller and G. Jackson, Annu. Rev. Chem. Biomol. Eng. **5**, 405 (2014).
[162] A. Mejía, C. Herdes, and E.A. Müller, Ind. Eng. Chem. Res. **53**, 4131 (2014).
[163] A. Mejia, M. Cartes, H. Segura, and E.A. Müller, J. Chem. Eng. Data **59**, 2928 (2014).
[164] C.G. Aimoli, E.J. Maginn, and C.R.A. Abreu, J. Chem. Eng. Data **59**, 3041 (2014).
[165] C.G. Aimoli, E.J. Maginn, and C.R.A. Abreu, J. Chem. Phys. **141**, 134101 (2014).
[166] T. Lafitte, D. Bessieres, M.M. Pineiro, and J.L. Daridon, J. Chem. Phys. **124**, 024509 (2006).
[167] F. Martinez-Veracoechea and E.A. Muller, Mol. Simul. **31**, 33 (2005).
[168] W. Smith, Mol. Simul. **32**, 933 (2006).
[169] W.G. Hoover, Phys. Rev. A **31**, 1695 (1985).
[170] S. Nosé, J. Chem. Phys. **81**, 511 (1984).
[171] J. Rowlinson and F. Swinton, *Liquids and Liquid Mixtures*, 3rd ed. (Butterworth Scientific, London, 1982).
[172] L. Vega, E. de Miguel, L.F. Rull, G. Jackson, and I.A. McLure, J. Chem. Phys. **96**, 2296 (1992).
[173] A. Trokhymchuk and J. Alejandre, J. Chem. Phys. **111**, 8510 (1999).
[174] G.J. Gloor, G. Jackson, F.J. Blas, and E. de Miguel, J. Chem. Phys. **123**, 134703 (2005).
[175] J.G. Kirkwood and F.P. Buff, J. Chem. Phys. **17**, 338 (1949).
[176] R.W. Zwanzig, J. Chem. Phys. **22**, 1420 (1954).
[177] E. de Miguel and G. Jackson, J. Chem. Phys. **125**, 164109 (2006).
[178] E. de Miguel and G. Jackson, Mol. Phys. **104**, 3717 (2006).
[179] P.E. Brumby, A.J. Haslam, E. de Miguel, and G. Jackson, Mol. Phys. **109**, 169 (2011).
[180] H. Wang, C. Schütte, and P. Zhang, Phys. Rev. E **86**, 026704 (2012).
[181] A.A. Louis, J. Phys.: Condens. Matter **14**, 9187 (2002).
[182] N. Ramrattan, Ph. D. thesis, Imperial College London, 2013.
[183] N. Ramrattan, E.A. Müller, and A. Galindo, Mol. Phys. (2014). <DOI:10.1080/00268976.2015.1025112.>
[184] J.A. Barker and D. Henderson, J. Chem. Phys. **47**, 4714 (1967).
[185] E.W. Lemmon, M.O. McLinden and D.G. Friend in *Thermophysical Properties of Fluid Systems in NIST Chemistry WebBook, NIST Standard Reference Database Number 69*, edited by P.J. Linstrom and W.G. Mallard (National Institute of Standards and Technology, Gaithersburg MD). <http://webbook.nist.gov>.
[186] O. Lobanova, Ph. D. thesis, Imperial College London, 2014.
[187] G.J. Gloor, G. Jackson, F.J. Blas, E.M. del Rio, and E. de Miguel, J. Chem. Phys. **121**, 12740 (2004).
[188] G.J. Gloor, G. Jackson, F.J. Blas, E.M. del Rio, and E. de Miguel, J. Phys. Chem. C **111**, 15513 (2007).
[189] F. Llovell, N. Mac Dowell, F.J. Blas, A. Galindo, and G. Jackson, Fluid Phase Equilib. **336**, 137 (2012).
[190] O. Lobanova, C. Herdes, G. Jackson, and E.A. Müller, Submitted (2015).
[191] E.A. Müller and A. Mejía, J. Phys. Chem. Lett. **5**, 1267 (2014).
[192] J.M. Míguez, J.M. Garrido, F. J. Blas, H. Segura, A. Mejía, and M.M. Piñeiro, J. Phys. Chem. C **118**, 24504 (2014).
[193] P.E. Theodorakis, E.A. Müller, R.V. Craster, and O.K. Matar, Submitted (2015).
[194] P.E. Theodorakis, E.A. Müller, R.V. Craster, and O.K. Matar, Curr. Opin. Colloid Interface Sci. **19**, 283 (2014).
[195] E.E. Santiso, C. Herdes, and E.A. Müller, Entropy **15**, 3734 (2013).
[196] D. van der Spoel, P.J. van Maaren, and H.J.C. Berendsen, J. Chem. Phys. **108**, 10220 (1998).
[197] B. Hess and N.F.A. van der Vegt, J. Phys. Chem. B **110**, 17616 (2006).
[198] P.T. Kiss and A. Baranyai, J. Chem. Phys. **131**, 204310 (2009).
[199] S. Rahman, O. Lobanova, C. Correia-Braga, V. Raptis, E.A. Müller, G. Jackson, and A. Galindo, Submitted (2015).